IEEE Access
Multidisciplinary ⋮ Rapid Review ⋮ Open Access Journal

Received 23 March 2025, accepted 2 April 2025, date of publication 7 April 2025, date of current version 15 April 2025.

Digital Object Identifier 10.1109/ACCESS.2025.3558398

RESEARCH ARTICLE

The Influence of Higher-Order Disturbance Estimation on Wind Power Generation of WECS Using SMC With Sensorless Wind Speed Estimation

AHMAD BALA ALHASSAN, (Member, IEEE), AND TON DUC DO, (Senior Member, IEEE)
Department of Robotics and Mechatronics, School of Engineering and Digital Sciences, Nazarbayev University, Astana 010000, Kazakhstan

Corresponding author: Ton Duc Do (doduc.ton@nu.edu.kz)

This research was funded by the Science Committee of the Ministry of Science and Higher Education of the Republic of Kazakhstan with Grant no. AP23489542 and the Grant title 'Enhancing Magnetic Particle Imaging System Sensitivity and Image Quality for Targeted Cancer Diagnosis and Treatment'. This research was also funded by Nazarbayev University, Kazakhstan, through the Social Policy Grant Program with Grant no. 201705 SPG.

ABSTRACT The increasing demand for environmentally friendly, renewable, and clean energy sources as a substitute to fossil fuels, which emit greenhouse gases, continues to rise. Nonetheless, extracting the maximum wind power through the wind energy conversion system (WECS) hinges on accurately measuring the generator's reference speed and the aerodynamic torque. This paper introduces an approach using an exponential disturbance estimator to extract the WECS's maximum power by estimating aerodynamic torque (T_a) and wind speed (v). Unlike most existing literature that assumes the behavior of the torque to change slowly, this paper offers a thorough investigation of the impact of fast-varying T_a on WECS's power harnessing using observer-based super-twisting sliding mode control (STSMC). Simulation results of reduced-intensity, fast-varying, and extremely fast-varying wind speeds for the zero-order (ZO), first-order (FO), and second-order (SO) T_a estimations were investigated. Though the incorporation of higher-order estimations improved the speed tracking performance and increased the maximum power extraction by about 6.5% for extremely varying wind profiles (from 182.15 kW to 193.92 kW), the ZO estimation almost extracted the same amount of power for fast-changing wind speed (151.87 kW vs 152.08 kW), and low-intensity wind force (6.86 kW vs 6.89 kW). Ultimately, the analyses suggested that in scenarios where the wind speed is not extremely changing, the ZO estimation proves effective, as the higher-order estimations will increase noise and the computational burden on the WECS.

INDEX TERMS Disturbance observer, renewable energy sources, sensorless wind speed estimation, wind energy conversion system (WECS).

I. INTRODUCTION

The extensive reliance on fossil fuels for global energy needs has raised significant environmental concerns due to the resulting impact on global warming. This is evident as a quarter of the global population lives in isolated villages where they use fossil fuels to meet their energy demand [1], [2]. Interestingly, the international community, particularly research institutions and other nonprofit organizations, is focusing considerably on cleaner, environmentally friendly, and renewable alternative energy sources. Therefore, due to their emission-free features, renewable energy sources such as biomass, hydro, wind, and sunshine (solar) are becoming increasingly popular [3], [4], [5].

Wind energy is among the cleanest and safest techniques for generating renewable electrical energy. Moreover, the environmental impact of wind energy generation is considerably lower or even negligible compared to other conventional

The associate editor coordinating the review of this manuscript and approving it for publication was Jorge Esteban Rodas Benítez.

energy sources. According to the latest international wind report [6], the new installations of wind farms, both onshore and offshore, reached 78 GW in 2022 alone, marking a significant increase of 54% from the 51 GW recorded in 2018. Therefore, this substantial increase highlights the increasing demand and extensive adoption of wind energy generation globally. On the other hand, most of the renewable energy sources are isolated in a stand-alone configuration, and it is crucial to integrate them into the grid for optimal power utilization. Some of the grid-forming methods were presented in [7], [8], [9], and [10]. However, the integration requires advanced controllers that can mitigate the effect of transient conditions, voltage fluctuations, and frequency mismatch, among others. For instance, Selvam et al. [11] proposes a novel distribution static compensator (DSTATCOM) for the distributed power of WECS. The adaptive schemes stabilize the grid parameters and reduce the total harmonic distortion (THD) under different load conditions. In [12], the validation of grid-integrated WECS was presented using the hardware in the loop (HIL) setup. The configuration shows that the DC-link voltage was effectively controlled with high integration efficiency.

Moreover, achieving efficient electrical power generation from wind sources depends heavily on the effective design, control, and regular maintenance of the electronic component for wind energy conversion. Therefore, extracting the maximum energy from the wind depends on effective control of the conversion method [13]. The control of wind energy conversion systems (WECSs) [14], [15], [16], [17], which is the most prominent component in wind energy harnessing, is crucial for efficient renewable energy production. Moreover, it is essential to note that at every time instants of varying wind profiles, there is an optimum point for the turbine to harness the maximum available power. Interestingly, this power can be harnessed by adjusting the generator's rotor voltage [18]. Nevertheless, the inherent nonlinearities of the WECS make its control challenging. Currently, the main types of generators for WECS integration include permanent magnet synchronous generators (PMSGs), doubly fed induction generators (DFIGs) [19], and synchronous reluctance generators (SynRGs) [20]. In this study, the PMSG, which is the most popular generator for the WECS, is considered.

Although the model of the WECS is needed for the control design, the uncertainties from the system modeling need to be effectively controlled. In [21], the dynamic modeling and control for WECS under parametric uncertainties was presented. Ayenew et al. [22] investigated the impact of uncertainties on the power extraction of WECS. The authors developed a control method that stabilizes the WECS. Also, Mohapatra and Dash [23] proposes a parametric disturbance rejection mechanism. In [24], the study addresses the impact of varying the parametric uncertainties of the WECS using an adaptive mechanism. However, the adaptive mechanism is complex and slows down the control action. In other studies, the intelligent and model predictive controllers [25], [26], [27] have been designed to enhance the performance of the WECS. These studies focused on uncertainties, highlighting the need for robust control design, which is employed in this study.

On the other hand, achieving optimal control of WECS depends on knowing the generator's reference speed, which is proportional to the wind speed. Unfortunately, conventional methods like cup anemometers could not satisfactorily measure the wind speed, especially for a fast-varying wind profile [28]. Other methods like the predictive algorithms [29], [30], [31], [32] have been employed to estimate the wind speed. However, their performance has often been unsatisfactory or limited to short-term predictions, and they involve intensive computations. Therefore, considering the challenges in accurately measuring wind speed, effective wind measurement is needed. For instance, in [33], a generalized high-order disturbance observer (GHODO) was designed for precise estimation of the wind speed. In another study [34], a variable structure system was proposed for a fixed pitch-based PMSG in varying wind conditions. In [35] and [36], the approach involves synthesizing a polynomial disturbance estimator capable of calculating the reference wind speed and aerodynamic torque. It is worth noting that the generator's shaft speed depends on the accurate measurement of the wind speed, which is related to the torque. However, in all the disturbance-observer-based studies, the torque is either assumed to be slowly varying or fast-changing without providing an in-depth analysis of the assumptions. Therefore, to our knowledge, none of the existing research analyzes the impact of higher-order disturbance estimation on the power generated from the WECS.

Therefore, this study aimed to conduct a comprehensive analysis of the effects of disturbance estimation using zero-order (ZO), first-order (FO), and second-order (SO) observers for a PMSG-based WECS. The study is an extended version of the paper presented at the IEEE conference on smart grid and renewable energy (SGRE2024) [37]. The concept, analysis, and results were extended and comprehensively presented. As the aerodynamic torque (T_a) is challenging to measure, the exponential disturbance observer (EDO) and higher-order EDO (HOEDO) were designed by assuming the torque to be a mismatched disturbance. As comprehensively presented in the recent review of the applications and trends of the WECS [38], the SMC, which has many variants, has demonstrated a superior performance over the existing control schemes. Thus, the super-twisting SMC (STSMC), with its excellent features including finite-time convergence, robustness to disturbance, and parametric uncertainties, was considered in this study. The STSMC was designed to regulate the d-axis current and to track the reference shaft speed. The STSMC incorporated the observers to study the influence of the order of disturbance for power extraction. Therefore, three cases of the wind profile were studied and analyzed. The response of the normal wind profile was recorded, and then its frequency was increased threefold, and finally, its amplitude

was decreased by one-third. These scenarios allowed the effects of changing the wind profile to be fully studied.

The contribution of the paper can be summarized as follows:

1) In most of the previous analyses (e.g., [28], [34]), the torque disturbance is considered to be slowly changing while neglecting the higher-order disturbance (HOD), and only one wind profile was chosen. In this study, the HOD was estimated using three different wind speeds ranging from medium to extremely fast-varying profiles.
2) Other studies that considered the disturbance to be fast-varying (e.g., [33], [39], [40]) only analyzed the estimation error of the ZO torque using the HOD estimation. Herein, the ZO, FO, and SO disturbances were incorporated into the controller, and their influence was analyzed for torque estimation, shaft-speed tracking, and most importantly, power extraction.
3) The observer' convergence and the stability assessment of the designed control system with the observer were guaranteed using the Lyapunov function. In comparison with an optimal control (LQR) [39], the proposed HOEDO-based STSMC has improved the disturbance estimation and the speed tracking by more than 50% in each case.
4) The study covers the possible operating wind profiles of the WECS and provides insight into the applicability of the HODO for the optimal operation of the WECS.

The overall content of the work is divided into seven sections. Section II describes the brief description and mathematical modeling of the PMSG-based WECS. Section III discusses the control design and the corresponding stability assessment. Section IV presents the exponential disturbance estimators. Section V presents the simulation results and analysis, while Section VI summarizes the discussions of the results. Finally, Section VII discusses the conclusion of the whole study.

II. SYSTEM DESCRIPTION AND MATHEMATICAL MODELLING

The process of converting wind sources to electrical energy can be achieved in two main phases. Firstly, the wind source is converted through aerodynamic coupling into mechanical energy. Finally, the electrical energy is generated via the mechanical coupling of the turbine blades connected to the electric generator. The dynamic modelling of the WECS in [39] is summarized and presented in this section to provide a better understanding of the control objectives of this research.

A. GENERATOR MODELLING

The magnitude of wind power can be represented in (1), where P_a denotes the aerodynamic wind power, ρ denotes the density of the air, R is the turbine radius, and v is the speed of the wind. The term $C_p(\lambda, \beta)$ is the power drag coefficient, which depends on the tip-speed ratio, λ, and blade pitch angle, β [39].

$$p_a = \frac{1}{2}\rho\pi R^2 C_p(\lambda, \beta)v^3 \tag{1}$$

Then, the λ can be determined using (2), where the given ω_t is the wind turbine speed. Then, the torque, T_a, can be illustrated in (3) by substituting (2) into (1).

$$\lambda = \frac{\omega_t}{v}R \tag{2}$$

$$T_a = \frac{p_a}{\omega_t} = \frac{1}{2}\rho\pi R^3 \frac{C_p(\lambda, \beta)}{\lambda}v^2 \tag{3}$$

As shown in (1), it is evident that the P_a depends on the power coefficient (C_p). It was studied that for different β, there is an optimal, λ such that $C_p(\lambda, \beta)$ is maximum. This scenario can be demonstrated in Fig. 1 using the typical formulation of (4) [41].

$$\begin{cases} C_p(\lambda, \beta) = \dfrac{1}{2}\left(\dfrac{116}{\Gamma_D} - 0.4\beta - 5\right)e^{-\left(\frac{21}{\Gamma_D}\right)}; \\ \dfrac{1}{\Gamma_D} = \left(\dfrac{1}{\lambda + 0.088\beta}\right) - \left(\dfrac{0.035}{\beta^3 + 1}\right) \end{cases} \tag{4}$$

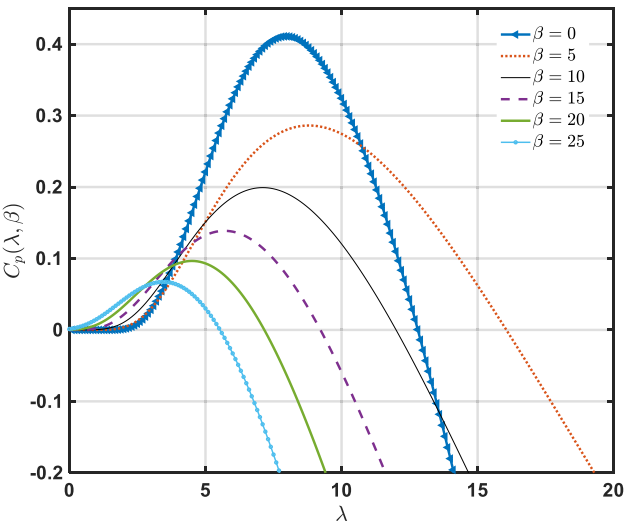

FIGURE 1. The relationship between the turbine's pitch angle, β and power coefficient, C_p, for different tip-speed-ratio, λ.

Therefore, the maximum P_a can be determined at the optimal λ (λ_{opt}) when C_p is at its peak. Remarkably, for a specific angle of the blade, the λ_{opt} is constant, which allows the harnessed power to be maximized by following the optimal speed reference of the turbine, ω_{ref}, as shown in (5) [39].

$$\omega_{ref} = \frac{\lambda_{opt}}{R}v \tag{5}$$

Also, considering the generator to be the PMSG with no gear connection, the dynamic model can be expressed as [39]:

$$\begin{cases} J\dfrac{d\omega(t)}{dt} = -B\omega(t) + T_a(t) - T_e(t) \\ \dfrac{di_q(t)}{dt} = -\dfrac{Rs}{L}i_q(t) - N_P\omega(t)i_d(t) - \dfrac{\psi_m N_P}{L}\omega(t) + \dfrac{1}{L}v_q(t) \\ \dfrac{di_d(t)}{dt} = -\dfrac{Rs}{L}i_d(t) + N_P\omega(t)i_q(t) + \dfrac{1}{L}v_d(t) \end{cases} \tag{6}$$

Additionally, the electromagnetic torque, $T_e(t)$ of (6), can be calculated using the relation [39]:

$$T_e(t) = Ki_q(t) \tag{7}$$

where $K = 3\psi_m N_P/2$. Thus, the overall modelling of the PMSG-based WECS considering the dynamics of the wind turbine can be established in (8) [39]. Finally, the generated power can be calculated as the product of torque (T_e) and the shaft angular speed (ω). The $C_p(\lambda, \beta)$ is commonly calculated experimentally based on β and λ of the wind turbine, and it is usually provided by the wind turbine's company (manufacturer). For fair performance comparison, the parameters of PMSG-based WECS presented in [39], as shown in Table 1, are adopted in this study. Similarly, the same parameters were adopted in [28], [33], [35], and [36].

$$\begin{cases} \dfrac{d\omega(t)}{dt} = -\dfrac{B}{J}\omega(t) - \dfrac{1}{J}T_e(t) + \dfrac{1}{J}T_a(t) \\ \dfrac{dT_e(t)}{dt} = -\dfrac{R_s}{L}T_e(t) - N_P K\omega(t)i_d(t) - \dfrac{\psi_m N_P K}{L}\omega(t) + \dfrac{K}{L}v_q(t) \\ \dfrac{di_d(t)}{dt} = -\dfrac{R_s}{L}i_d(t) + \dfrac{N_P}{K}\omega(t)T_e(t) + \dfrac{1}{L}v_d(t) \end{cases} \tag{8}$$

TABLE 1. Parameters of PMSG-based WECS.

S/N	Symbol	Parameter	
1	R	Radius of rotor	1.84 m
2	N_P	Number of pole pairs	14
3	L_s	Nominal stator inductance	3.55 mH
4	R_s	Nominal stator resistance	0.3676 Ω
5	B_v	Coefficient of viscous friction	0.002 kg.m^2/s
6	J	Equivalent rotor inertia	7.856 kg.m^2
7	ψ_m	Magnitude flux linkage	0.2867 V.s/rad
8	λ_{opt}	Maximum tip-speed ratio	8.1
9	C_{p_max}	Maximum power coefficient	0.3262
10	ρ	Air density	1.25 kg/m^3

B. PROBLEM FORMULATION AND OBJECTIVES

As earlier stated, achieving optimal control of WECS depends on knowing the generator's reference speed, which is proportional to the wind speed. Unfortunately, conventional methods like cup anemometers could not satisfactorily measure the wind speed, especially for a fast-varying wind profile. According to the structure of the WECS, the following assumptions for the mathematical modeling and control of the WECS were formulated:

i. The angular speed of the generator (ω), T_e, i_q, and i_d are available (measurable).
ii. The torque (T_a) and the wind speed (v) are unknown and, therefore, need to be observed or estimated.

It is hypothesized that information on the torque estimation and the corresponding wind speed can be obtained using disturbance observers since the torque acts as an external disturbance to the system. Secondly, optimal power can be harnessed if the shaft speed is controlled effectively so that it follows the reference wind speed. However, this can only be achieved by efficient T_a estimation and robust shaft speed control.

In most current research, $T_a(t)$ was considered to be slowly varying. Nonetheless, the studies failed to validate their assumptions through a comparative analysis of the impact of higher-order torque estimation on power harnessing. Thus, the objective of this study is to examine the effects of torque disturbance estimation on shaft-speed tracking and power extraction, specifically focusing on ZO, FO, and SO torques. The robust STSMC will be designed for the shaft speed control, and a HOEDO will be designed to investigate the influence of different orders of torque estimation on shaft speed tracking and power generation.

III. CONTROL DESIGN

Before designing the controllers, it is important to highlight that the surface-mounted type of the PMSG is being considered. Consequently, the d-axis current should be controlled to zero for effective automation of the system. In this context, two primary control objectives were recommended:

i. *d-axis current control*: The objective here is to maintain the current (i_d) to zero by regulating the d-axis voltage (v_d)
ii. *Speed tracking*: In this case, the objective is to control q-axis voltage (v_q) such that the shaft speed (ω) follows the reference speed (ω_{ref}).

The SMC/STSMC is employed to accomplish the stated objectives; SMC ensures robust control within a sliding mode manifold, where the output response precisely follows the desired reference trajectory. The controller was chosen due to its proven reputation for good regulation action and tracking control for many control systems. The typical SMC's action is demonstrated in Fig. 2 and (9) [42], where the sliding surface (Ψ_s) forced the system states from the initial point (x_{t0}) to track the desired trajectory. The sliding surface coefficient (γ_s) determines the speed of convergence of the tracking error. In this study, the robust STSMC was designed and compared with the traditional SMC.

$$\Psi_s = \gamma_s e(t) + \dot{e}(t);\ \gamma_s \geq 0 \tag{9}$$

A. CONVENTIONAL SMC

1) d-axis voltage Control (V_d)

According to the stated objective, the goal is to regulate the d-axis current to zero for the surface-mounted-based PMSG.

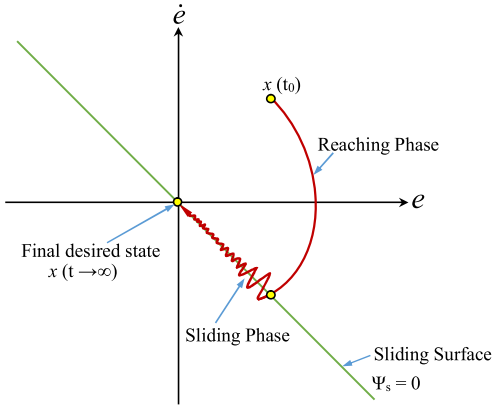

FIGURE 2. The mechanism of sliding mode control (SMC).

Thus, the sliding surface for the current control is expressed in (10), where the reference signal $i_{dr} = 0$, Δ_{cc} represents a positive gain. Then, the derivative of (10) can be simplified in (11) using the third part of (8).

$$\Psi^s_{id}(t) = \Delta_{cc}\left(i_d(t) - i_{dr}(t)\right); \Delta_{cc} > 0 \tag{10}$$

$$\begin{aligned}\dot{\Psi}^s_{id}(t) &= \Delta_{cc}\dot{i}_d(t)\\ &= \Delta_{cc}\left(-\frac{Rs}{L}i_d(t) + \frac{N_P}{K}\omega(t)T_e(t) + \frac{1}{L}v_d(t)\right)\end{aligned} \tag{11}$$

Moreover, the reaching law for the i_d is chosen as in (12), where β_1 and β_2 are the positive switching gains. Finally, the control law, $v_{dSM}(t)$, comprising the switching control and equivalent control, can be expressed in (13) by equating (11) and (12):

$$\dot{\Psi}^s_{id}(t) = \beta_1 sign\left(\Psi^s_{id}(t)\right) - \beta_2\Psi^s_{id}(t); \beta_1,\ \beta_2 > 0 \tag{12}$$

$$\begin{aligned}v_{dSM}(t) = R_s i_d(t) &- \frac{N_P L}{K}\omega(t)T_e(t) - \frac{L}{\Delta_{cc}}\beta_1 sign\left(\Psi^s_{id}(t)\right)\\ &- \frac{L}{\Delta_{cc}}\beta_2\Psi^s_{id}(t)\end{aligned} \tag{13}$$

2) q-axis voltage Control (v_q) for shaft speed tracking (ω)

The objective of the $v_q(t)$ control is to force the shaft speed, $\omega(t)$, to follow the reference ω_{ref} ,as shown in (14). To achieve this objective, the sliding surface $\Psi^s_\omega(t)$ of (15) was chosen for a given positive gain ξ_ω.

$$\tilde{\omega}(t) = \omega_{ref}(t) - \omega(t) \tag{14}$$

$$\Psi^s_\omega(t) = \dot{\tilde{\omega}}(t) + \xi_\omega\tilde{\omega}(t); \xi_\omega > 0 \tag{15}$$

Moreover, considering the HO derivative of the reference tracking, the derivative of (15) is expressed in (16) and simplified into (17) using (8):

$$\begin{aligned}\dot{\Psi}^s_\omega(t) &= \ddot{\tilde{\omega}}(t) + \xi_\omega\dot{\tilde{\omega}}(t) = \ddot{\omega}_{ref}(t) + \xi_\omega\dot{\omega}_{ref}(t)\\ &\quad - \ddot{\omega}(t) - \xi_\omega\dot{\omega}(t)\\ \dot{\Psi}^s_\omega(t) &= \ddot{\omega}_{ref}(t) + \xi_\omega\dot{\omega}_{ref}(t)\\ &\quad - \left(\frac{B}{J}\Gamma + \frac{\psi_m N_P K}{JL}\right)\omega(t) - \frac{1}{J}\dot{T}_a(t)\end{aligned} \tag{16}$$

$$\begin{aligned}&- \left(\frac{R_s}{JL} + \frac{\Gamma}{J}\right)T_e(t) - \frac{N_P K}{J}\omega(t)i_d(t) + \frac{\Gamma}{J}T_a(t)\\ &+ \frac{K}{JL}v_q(t)\end{aligned} \tag{17}$$

where $\Gamma = (B/J)$ - ξ_ω. Also, the switching law of (18) was chosen for the given switching gains η_1 and η_2. Finally, the overall control law, $v_{qSM}(t)$, comprising the switching and equivalent controls, can be determined by equating (17) and (18) as illustrated in (19):

$$\dot{\Psi}^s_\omega(t) = -\eta_1 sign\left(\Psi^s_\omega(t)\right) - \eta_2\Psi^s_\omega(t); \eta_1,\ \eta_2 > 0 \tag{18}$$

$$\begin{aligned}v_{qSM}(t) = &\left(\frac{BL}{K}\Gamma + \psi_m N_P K\right)\omega(t) + \left(\frac{R_s}{K} + \frac{\Gamma L}{K}\right)T_e(t)\\ &+ N_P L\omega(t)i_d(t) - \frac{\Gamma L}{K}T_a(t) + \frac{L}{K}\dot{T}_a(t) - \frac{JL}{K}\ddot{\omega}_{ref}(t)\\ &- \frac{JL}{K}\xi_\omega\dot{\omega}_{ref}(t) - \frac{JL}{K}\eta_1 sign\left(\Psi^s_\omega(t)\right) - \frac{JL}{K}\eta_2\Psi^s_\omega(t)\end{aligned} \tag{19}$$

B. HIGHER-ORDER SMC (SUPER-TWISTING)

In this section, the super-twisting SMC (STSMC), one of the higher-order SMCs, is considered for the comparative analysis. Obviously, the sign function related to switching conditions of the SMC can cause chattering, which can have a negative impact on the performance of the control system. Although some improvements were made regarding the performance of the traditional SMC, introducing STSMC is a game changer as it does not require much information on the system, and it minimizes the chattering effect by making the control action continuous instead of the discontinuous behavior of the SMC [42]. Thus, the STSMC can be designed and implemented effectively with details of the sliding surface of the previously designed SMC of (13) and (19). Hence, after simplifications, the control signals $v_{dST}(t)$ and $v_{qST}(t)$ for the $i_d(t)$ regulation and $\omega(t)$ tracking were determined as:

$$v_{dST}(t) = R_s i_d(t) - \frac{N_P L}{K}\omega(t)T_e(t) + \frac{L}{\Delta_{cc}}C_{DST} \tag{20}$$

$$\begin{aligned}v_{qST}(t) = &\left(\frac{BL}{K}\Gamma + \psi_m N_P K\right)\omega(t) + \left(\frac{R_s}{K} + \frac{\Gamma L}{K}\right)T_e(t)\\ &+ N_P L\omega(t)i_d(t) - \frac{\Gamma L}{K}T_a(t) + \frac{L}{K}\dot{T}_a(t) - \frac{JL}{K}\ddot{\omega}_{ref}(t)\\ &- \frac{JL}{K}\xi_\omega\dot{\omega}_{ref}(t) + \frac{JL}{K}C_{QST}(t)\end{aligned} \tag{21}$$

where $C_{QST}(t)$ and $C_{DST}(t)$ are the switching terms of the STSMC for the $v_{qST}(t)$ and $v_{dST}(t)$, respectively, as derived from the standard STSMC configuration in [43]::

$$\begin{cases} C_{QST}(t) = -C_{Q1}\left|\Psi^s_\omega(t)\right|^{\delta_1} sign\left(\Psi^s_\omega(t)\right) - C_{Q2}\int sign\left(\Psi^s_\omega(t)\right)dt\\ C_{DST}(t) = -C_{D1}\left|\Psi^s_{id}(t)\right|^{\delta_2} sign\left(\Psi^s_{id}(t)\right) - C_{D2}\int sign\left(\Psi^s_{id}(t)\right)dt\\ C_{Q1}, C_{Q2}, C_{D1}, C_{D2} > 0; \end{cases}$$

In addition, the coefficients C_{Q1}, C_{Q2}, δ_1, δ_2, C_{D1}, and $C_{D2}$are the positive gains, which dictates the tracking performance and error convergence of the controller. To guarantee

the stability of the STSMC, the power terms should be between zero and 1 (i.e., $0 < (\delta_1, \delta_2) > 1$) as illustrated [42].

C. STABILITY ANALYSIS

1) d-axis voltage Control (V_d)

The v_d represents the d-axis component of the armature voltage, which is controlled via the d-axis component of the armature current (i_d) [44]. As highlighted earlier, since the PMSG is surface mounted, the $i_d(t)$ is maintained at zero by regulating the $v_d(t)$ as shown in Eq. (13). Thus, the stability analysis for $i_d(t)$ regulation can be assessed by selecting the Lyapunov function for the current control, $L_i^f(t)$ of (22) to reflect the sliding surface of (10). Then, the time derivative of the $L_i^f(t)$ was expressed in (23). Therefore, by substituting the control signal, $v_d(t)$ of (13) into (12), all the other terms except for the switching terms will be cancelled out (zero), leading to the simplified results of (23).

$$L_i^f(t) = \frac{1}{2}\left(\Psi_{id}^s(t)\right)^2 \tag{22}$$

$$\begin{aligned}\dot{L}_i^f(t) &= \Psi_{id}^s(t)\dot{\Psi}_{id}^s(t) = \Psi_{id}^s(t)\left(-\beta_1 sign\left(\Psi_{id}^s(t)\right) - \beta_2\Psi_{id}^s(t)\right)\\ &= -\beta_1\left|\Psi_{id}^s(t)\right| - \beta_2\left(\Psi_{id}^s(t)\right)^2 \le 0\end{aligned} \tag{23}$$

2) q-axis voltage control (v_q)

Similarly, V_q represents the q-axis component of the armature voltage, while $i_q(t)$ denotes the q-axis component of the armature current. The $v_q(t)$ is controlled to regulate the generator's shaft speed (ω). Thus, the stability of the system can be investigated by selecting the Lyapunov function for the v_q control as in (24) to reflect the sliding surface of (15). Then, the time derivative of the (24) was expressed in (25). Therefore, by substituting the control signal (19) into (17), all the other terms except for the switching terms will be cancelled out, leading to the simplified results of (25).

$$L_\omega^f(t) = \frac{1}{2}\left(\Psi_\omega^s(t)\right)^2 \tag{24}$$

$$\begin{aligned}\dot{L}_\omega^f(t) &= \left(\Psi_\omega^s(t)\right)\dot{\Psi}_\omega^s(t) = \Psi_\omega^s(t)\left(-\eta_1 sign\left(\Psi_\omega^s(t)\right) - \eta_2\Psi_\omega^s(t)\right)\\ &= -\eta_1\left|\Psi_\omega^s(t)\right| - \eta_2\left(\Psi_\omega^s(t)\right)^2 \le 0\end{aligned} \tag{25}$$

Remark 1: According to the Lyapunov stability theorem, the derivative of the selected Lyapunov function should be negative. Thus, considering the results of (23) and Eq. (25), it can be established that for any given positive switching gains (i.e., β_1, β_2, η_1,and η_2), the solutions would always be ≤ 0. Hence, the stability of the controllers for both the speed tracking ($\omega(t) \to \omega_{ref}$) and current control ($i_d(t) \to 0$) is guaranteed.

IV. EXPONENTIAL DISTURBANCE OBSERVER (EDO)

In this section, the ZO and HO disturbance estimators and their respective convergence assessments were discussed. Thus, to incorporate the estimations into the control system, the estimated terms would be utilized by re-arranging the control signal to include the estimated terms as:

$$\begin{aligned}v_q(t) = &\left(\frac{BL}{K}\Gamma + \psi_m N_P K\right)\omega(t) + \left(\frac{R_s}{K} + \frac{\Gamma L}{K}\right)T_e(t)\\ &+ N_P L\omega(t) i_d(t) - \frac{\Gamma L}{K}\hat{T}_a(t) + \frac{L}{K}\dot{\hat{T}}_a(t) - \frac{JL}{K}\ddot{\omega}_{ref}(t)\\ &- \frac{JL}{K}\xi_\omega\dot{\hat{\omega}}_{ref}(t) - \frac{JL}{K}\eta_1 sign\left(\Psi_\omega^s(t)\right) - \frac{JL}{K}\eta_2\Psi_\omega^s(t)\end{aligned} \tag{26}$$

where the wind speed ($v(t)$) is estimated from the estimated torque using (3). Thus, the corresponding reference speed can be expressed as in (27). It is worth noting that the derivative of the speed is with respect to time for varying wind profiles:

$$\begin{cases}\omega_{ref}(t) = \frac{\lambda_{opt}}{R}\hat{v}(t) \Rightarrow \hat{v}(t) = \sqrt{\frac{2\lambda_{opt}\hat{T}_a(t)}{(\rho\pi R^3 C_{p\max})}};\\ \dot{\omega}_{ref}(t) = \frac{\lambda_{opt}}{R}\dot{\hat{v}}(t) \Rightarrow \dot{\hat{v}}(t) = \frac{\lambda_{opt}\dot{\hat{T}}_a(t)}{(\rho\pi R^3 C_{p\max})\hat{v}(t)};\\ \ddot{\omega}_{ref}(t) = \frac{\lambda_{opt}}{R}\ddot{\hat{v}}(t) \Rightarrow \ddot{\hat{v}}(t) = \frac{\lambda_{opt}\ddot{\hat{T}}_a(t)}{\hat{v}(t)(\rho\pi R^3 C_{p\max})} - \left(\frac{\dot{\hat{v}}^2(t)}{\hat{v}(t)}\right)\end{cases} \tag{27}$$

A. ZERO-ORDER EXPONENTIAL DISTURBANCE OBSERVER (ZOEDO)

Using the concept of EDO [45], the $T_a(t)$ can be obtained from the first term of (8) as illustrated in (28). Thus, the ZOEDO can be represented in (29) based on the assumption that the $T_a(t)$ varies slowly. Then, the estimated torque can be represented in (30) by substituting (28) in (29).

$$T_a(t) = J\dot{\omega}(t) + B\omega(t) + T_e(t) \tag{28}$$

$$\dot{\hat{T}}_a(t) = \xi_o\left(T_a(t) - \hat{T}_a(t)\right); \xi_o > 0 \tag{29}$$

$$\dot{\hat{T}}_a(t) = \xi_o\left(J\dot{\omega}(t) + B\omega(t) + T_e(t)\right) - \xi_o\hat{T}_a(t) \tag{30}$$

Therefore, it can be established that given the measurements of acceleration, the $T_a(t)$ can be estimated. However, since the acceleration of the motor is generally difficult to measure, an auxiliary term, $\mu(t)$, and its derivative w.r.t are shown as:

$$\mu(t) = \hat{T}_a(t) - \xi_o J\omega(t) \tag{31}$$

$$\begin{aligned}\dot{\mu}(t) &= \xi_o\left(J\dot{\omega}(t) + B\omega(t) + T_e(t)\right) - \xi_o\hat{T}_a(t) - \xi_o J\dot{\omega}(t)\\ &= \xi_o\left(B\omega(t) + T_e(t)\right) - \xi_o\hat{T}_a(t)\end{aligned} \tag{32}$$

Finally, the estimator dynamics can be represented in (33) after solving for (32) and (30).

$$\begin{aligned}\hat{T}_a(t) &= \mu(t) + \xi_o J\omega(t)\\ \dot{\mu}(t) &= \xi_o(B\omega(t) + T_e(t) - \xi_o J\omega(t)) - \xi_o\mu(t)\end{aligned} \tag{33}$$

Convergence assessment 1: For the observers to be effevctive, the estimation error should converge to zero in a finite time. Thus, the estimation error is defined in (34), and its corresponding dynamics are illustrated in (35) for a slowly changing $T_a(t)$ using (28)- (31).

$$\tilde{T}_a(t) = T_a(t) - \hat{T}_a(t) \tag{34}$$

$$\begin{aligned}\dot{\tilde{T}}_a(t) &= -\xi_o(B\omega(t) + T_e(t) - \xi_o J\omega(t)) + \xi_o\mu(t) - \xi_o J\dot{\omega}(t)\\ &= -\xi_o(B\omega(t) + T_e(t) + J\dot{\omega}(t)) + \xi_o(\mu(t) + \xi_o J\omega(t))\\ &\Rightarrow \dot{\tilde{T}}_a(t) + \xi_o\tilde{T}_a(t) = 0\end{aligned} \tag{35}$$

Theorem 1: It is obvious that the final simplification of (35) is a 1st-order homogeneous DE whose solution of (36) will exponentially approach zero in finite time (i.e., $t \rightarrow \infty$) according to the magnitude of the estimation gain, ξ_o. In addition, the estimation error will be maximum at the initial time of estimation (i.e., t = t(0)), which quickly decays to zero.

$$\dot{\tilde{T}}_a(t) = \tilde{T}_a(t_0)e^{-\xi_o t};\ \left|\tilde{T}_a\right|_{\max} = \left|\tilde{T}_a\left(t_0\right)\right| \tag{36}$$

B. HIGHER-ORDER EXPONENTIAL DISTURBANCE OBSERVER (HOEDO)

Although the wind profile can be assumed to be slowly changing, in reality, it can be changing rapidly. Therefore, the ZEODO might not comprehensively represent the behavior of the observed torque. In this regard, the concept of HOEDO [46] is utilized to estimate the fast-changing T_a(t). According to the control law of (26), only the 2nd-order (SO) estimation of the estimated parameters is required. Thus, the SO HOEDO can be represented in (37) using (8), where μ_1(t), μ_2(t), and μ_3(t) are the auxiliary variables, and Υ_1^o, Υ_2^o, and Υ_3^o are the observer gains.

$$\begin{cases} \hat{T}_a(t) = \mu_1(t) + \Upsilon_1^o\omega(t) \\ \dot{\hat{T}}_a(t) = \mu_2(t) + \Upsilon_2^o\omega(t) \\ \ddot{\hat{T}}_a(t) = \mu_3(t) + \Upsilon_3^o\omega(t) \\ \dot{\mu}_1(t) = -\Upsilon_1^o\left(-\frac{B}{J}\omega(t) - \frac{1}{J}T_e(t) + \frac{1}{J}\hat{T}_a(t)\right) + \dot{\hat{T}}_a(t) \\ \dot{\mu}_2(t) = -\Upsilon_2^o\left(-\frac{B}{J}\omega(t) - \frac{1}{J}T_e(t) + \frac{1}{J}\hat{T}_a(t)\right) + \ddot{\hat{T}}_a(t) \\ \dot{\mu}_3(t) = -\Upsilon_3^o\left(-\frac{B}{J}\omega(t) - \frac{1}{J}T_e(t) + \frac{1}{J}\hat{T}_a(t)\right) \end{cases} \tag{37}$$

Convergence Assessment 2: Let the estimation error of the torque for the HO observer be defined in (38). Then, by simplifying the observer dynamics of (37) using (8) and (38), the estimation error equation can be represented in (39).

$$\tilde{T}_1 = T_a - \hat{T}_a\ ;\ \ \tilde{T}_2 = \dot{T}_a - \dot{\hat{T}}_a\ ;\ \ \tilde{T}_3 = \ddot{T}_a - \ddot{\hat{T}}_a \tag{38}$$

$$\begin{cases} \dot{\tilde{T}}_1(t) = \tilde{T}_2(t) - \frac{\Upsilon_1^o}{J}\tilde{T}_1(t) \\ \dot{\tilde{T}}_2(t) = \tilde{T}_3(t) - \frac{\Upsilon_2^o}{J}\tilde{T}_1(t) \\ \dot{\tilde{T}}_3(t) = -\frac{\Upsilon_3^o}{J}\tilde{T}_1(t) \end{cases} \Rightarrow \begin{bmatrix} \dot{\tilde{T}}_1(t) \\ \dot{\tilde{T}}_2(t) \\ \dot{\tilde{T}}_3(t) \end{bmatrix}$$

$$= \begin{bmatrix} -\frac{\Upsilon_1^o}{J} & 1 & 0 \\ -\frac{\Upsilon_2^o}{J} & 0 & 1 \\ -\frac{\Upsilon_3^o}{J} & 0 & 0 \end{bmatrix} \begin{bmatrix} \tilde{T}_1(t) \\ \tilde{T}_2(t) \\ \tilde{T}_3(t) \end{bmatrix} \tag{39}$$

Theorem 2: Considering the error matrix of (39), the characteristics polynomial can obtained in (40). Thus, if the estimation gains (Υ_1^o, Υ_2^o, and Υ_3^o) are selected such that (40) is Hurwitz [47], the torque estimations errors will asymptotically approach zero in finite time (i.e., $t \rightarrow \infty$).

$$s^3 + \Upsilon_1^o s^2 + \Upsilon_2^o s + \Upsilon_3^o = 0 \tag{40}$$

C. CLOSED-LOOP STABILITY ANALYSIS WITH OBSERVERS

Since the current regulation of (13) does not include any estimated parameter, the stability analysis of (23) still holds. However, the stability analysis of the speed tracking needs to be re-assessed with the observers. Thus, by substituting the closed-loop control law of (26) into (17), the switching surface can be re-arranged by incorporating the observers as:

$$\dot{\Psi}_\omega^s(t) = \frac{\Gamma}{J}\tilde{T}_a(t) - \frac{1}{J}\dot{\tilde{T}}_a(t) - \eta_1 sign\left(\Psi_\omega^s(t)\right) - \eta_2\Psi_\omega^s(t) \tag{41}$$

Therefore, the Lyapunov function, $L_{OC}(t)$ of (42), is selected to reflect the dynamics of (41). Then, its corresponding derivative w.r.t can be simplified in (43) after incorporating the estimation error dynamics of (34). Thus, since the system is governed by two control signals (v_d and v_q), the stability analysis of (23) and (43) represents the stability assessment of the complete closed-loop control system.

$$L_{OC}(t) = \frac{1}{2}\left(\Psi_\omega^s(t)\right)^2 + \frac{1}{2}\tilde{T}_a^2(t) \tag{42}$$

$$\begin{aligned} \dot{L}_{OC}(t) &\leq \Psi_\omega^s(t)\dot{\Psi}_\omega^s(t) + \tilde{T}_a\dot{\tilde{T}}_a(t) \\ &= \Psi_\omega^s(t)\left(-\eta_1 sign\left(\Psi_\omega^s(t)\right) - \eta_2\Psi_\omega^s(t) + \left(\frac{\xi_o}{J} + \frac{\Gamma}{J}\right)\tilde{T}_a\right) \\ &\quad + \tilde{T}_a\left(-\xi_o\tilde{T}_a\right) \\ &= -\eta_1\left|\Psi_\omega^s(t)\right| - \eta_2\left(\Psi_\omega^s(t)\right)^2 + \left(\frac{\xi_o}{J} + \frac{\Gamma}{J}\right)\tilde{T}_a\Psi_\omega^s(t) \\ &\quad - \xi_o\tilde{T}_a^2 \leq 0 \end{aligned} \tag{43}$$

Remark 2: To guarantee the stability of the control system with the observers, the summation of the three negative terms of (43) should be greater than the remaining single positive term. Although this would always be the case considering the magnitude of the negative terms, stability can be assured if any of the gains or summation of the gains is greater than the gain of the positive term, as illustrated in (44). Additionally, since the observers were initially designed such that the

estimation error decays in finite time, the closed-loop system with the observers will always be stable:

$$either\ [\eta_1, \eta_2, (\eta_1+\eta_2)] \geq \begin{cases} \left(\frac{\xi_o}{J}+\frac{\Gamma}{J}\right)\left|\tilde{T}_a\right|_{\max} \\ or \\ \left(\frac{\xi_o}{J}+\frac{\Gamma}{J}\right)\left|\tilde{T}_a(0)\right| \end{cases} \quad (44)$$

V. RESULTS AND ANALAYSIS

The simulation analysis was conducted using the PMSG-based WECS of (8), SMC/STSMC of (13) and (19)-(21)), observers of (33) and (37), and the parameters of Tables 1 and 2 in Matlab/Simulink. As shown in Fig. 3, the disturbance observer (HEODO) estimates the torque generated by the wind force acting on the turbine blades and the corresponding reference speeds. Thus, the torque serves as the input to the system, while the reference speed is used as the reference to the control (sliding surface). Hence, the torque only serves as an input for the control, not a disturbance that needs to be rejected or compensated for.

The profile of the wind was generated using (45) [48], where v_a and v_f, respectively, represent the magnitude and frequency of the wind profile, $v(t)$. In [48], the wind profile has constant parameters, i.e. there was no v_a ($v_a = 1$), and v_f was $= 0.0625$. In our case, the v_a and v_f were introduced so that the profile can be varied. Thus, three different wind profiles were generated, namely, CASE I ($v_a = 1$ and $v_f = 0.0625$), CASE II ($v_a = 1$ and $v_f = 3{*}0.0625$), and CASE III ($v_a = 1/3$ and $v_f = 0.0625$), which allows for a comprehensive analysis of the impact of the varying torque estimations. Finally, the authors generated the observer and control gains of Table 2, which are constant values. Some researchers use trial and error to get the gains. However, in this study, we use the built-in Matlab®gradient descent optimization toolbox to get the best values of the gains.

$$v(t) = v_a \begin{pmatrix} 10 + 0.55(\sin(0.2\pi v_f t) - 0.875\sin(0.6\pi v_f t) \\ +0.75\sin(\pi v_f t) - 0.625\sin(2\pi v_f t) \\ -0.5\sin(6\pi v_f t) + 0.25\sin(10\pi v_f t) \\ +0.125\sin(20\pi v_f t)) \end{pmatrix} \quad (45)$$

TABLE 2. Simulation parameters.

Parameter	Symbol
ZOEDO	$\xi_0 = 100$
HOEDO	$\Upsilon^o_1 = 3000$; $\Upsilon^o_2 = 20000$; $\Upsilon^o_3 = 50000$
SMC (V_{qSM})	$\eta_1 = 500$; $\eta_2 = 2.5$; $\xi_\omega = 50$
SMC (V_{dSM})	$\beta_1 = 1$; $\beta_2 = 1$; $\beta_{cc} = 1$
STSMC (V_{qST})	$C_{D1} = 1$; $C_{D2} = 20$; $\delta_1 = 0.50$
STSMC (V_{dST})	$C_{Q1} = 1$; $C_{Q2} = 25$; $\delta_2 = 0.50$

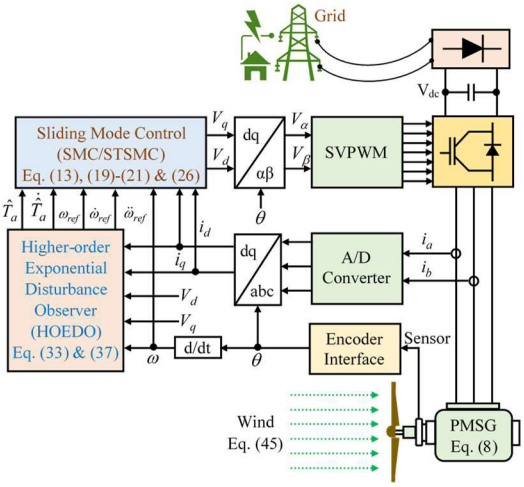

FIGURE 3. The schematic representation of the proposed HOEDO-based SMC for the control of WECS.

A. CONTROL OBJECTIVES WITH VARYING WIND PROFILE

To compare the performance of the started control objectives, different cases of the wind profiles were generated from the formulation of (45) based on various characteristics of the wind profile. The analyses would allow for a better understanding of the influence of wind profile for maximum power harnessing of the WECS and to assess the effectiveness of the designed control system.

CASE I: Here, the control system's response under normal wind speed is analyzed using the original values of the wind magnitude (v_a) and frequency (v_f), i.e., $v_a = 1$ and $v_f = 0.0625$.

CASE II: In this scenario, the frequency of the wind profile is increased threefold ($3{*}\ v_f$). Thus, the response of the wind profile will be extremely varying.

CASE III: Finally, the magnitude of the wind profile was decreased to one-third ($v_a/3$), which represents a reduced intensity of the wind source.

Figure 4(a) shows the behavior of the three selected wind profiles for the performance analysis of the control system. Then, these wind profiles were applied to the system as an input. The responses for the stated control objectives, namely, the d-axis current control and the reference shaft speed tracking, were recorded. The response of the current regulation has achieved the stated aim of maintaining the d-axis current within zero in all cases. Moreover, the shaft speed tracking is controlled effectively to follow the behavior of the wind profiles, as illustrated in Fig. 4(b). The shaft speed is proportional to the intensity of the wind profiles. These responses demonstrated that the controller was effectively designed and could be applied to investigate the influence of a higher-order disturbance estimator.

B. PERFORMANCE OF TORQUE DISTURBANCE ESTIMATION

The torque disturbance was estimated using ZOEDO and HOEDO of (33) and (37). The ZOEDO only estimates

zero-order disturbance (ZO), while the HOEDO estimates the ZO, first-order (FO), and second-order (SO) disturbances. The main aim of the study is to investigate the influences of all the observers on the performance of the WECS. Figure 5 shows the response of the disturbance estimation for the three wind profiles using both ZOEDO and HOEDO. As shown in Fig. 5(a)-(c), it is obvious that both observers follow the actual torque satisfactorily.

Furthermore, the corresponding estimation errors (e_{Ta}) for the three scenarios are illustrated in Fig. 5 (d)-(f). As shown, the observers estimate the disturbance very well with minimal error. Nonetheless, the HOEDO has the least error, ranging from 0.005 to 0.4 N.m, compared to the ZOEDO, which has 0.07 to 2 N.m for low wind amplitude and very fast wind, respectively. Also, as the dynamics of (36) dictates, the error (e_{Ta}) was maximum at the initial time (i.e., t = 0), which exponentially decays to zero.

In addition, Fig. 5 (g)-(i) shows the response of the FO torque estimation using the HOEDO for the three different wind profiles. The HOEDO estimates the FO disturbance satisfactorily. In all cases, the maximum error occurs at the initial application of the observer. It is also clear that the initial estimation error is higher for increased wind speed. Moreover, the second-order (SO) estimations are illustrated in Fig. 5 (j)-(l). As shown in Fig. 7(k), the SO torque can reach up to 400 N.m for a very fast wind profile, which could have a significant impact on the control system. Thus, the notion that the HO torque is negligible should not be generalized.

C. INFLUENCE OF ZOEDO AND HOEDO ON THE SHAFT SPEED (ω) AND MAXIMUM POWER EXTRACTION

In the previous section, the performance of the observers was analyzed for the three different cases of wind profiles. In this section, the influence of the order of the estimation on the shaft speed (ω) tracking and the power extraction is analyzed using the designed controllers. Figure 6(a)-(c) and (d)-(f) shows the response of the ω(t) tracking for the three wind profiles, respectively, for the SMC and STSMC. As shown, SO+FO+ZO represents the response after incorporating ZO, FO, and SO estimations into the controller, whereas FO+ZO illustrated that the SO estimation was not considered. Finally, ZO shows the response of using only the ZO estimations. Thus, the results demonstrate the impact of adding HO estimations to the control system. Also, the corresponding tracking errors are illustrated in Fig. 6(g)-(i) and (j)-(l). It is evident that the addition of the SO estimations has no significant influence on the speed tracking. However, using ZO only increases the tracking error. Similarly, the corresponding power extraction is illustrated in Fig. 7.

D. PERFORMANCE COMPARISON OF SMC, STSMC, AND LQR

The preceding analyses investigated the performance of the proposed EDO-based SMC and STSMC in detail. However, to assess the effectiveness of the scheme, a comparative study with other controllers should be presented. The LQR is a

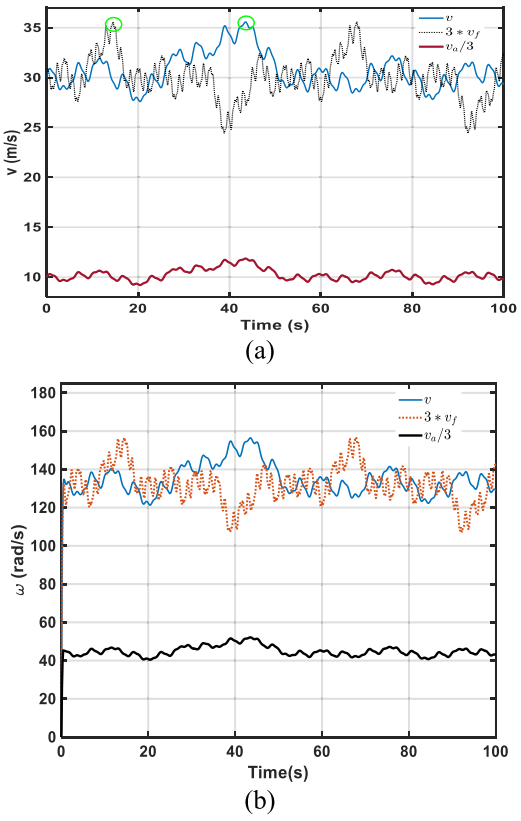

FIGURE 4. (a) The three generated wind profiles from (45) by increasing the wind frequency (v_f) and magnitude (v_a), respectively; (b) The response of angular shaft speed (ω), which effectively follows the given wind profiles.

crucial control approach that ensures the optimal behavior of a dynamic system by minimizing a specific cost function. As the name implies, LQR minimizes a quadratic cost function and uses a linear state-space model for its design. A typical linear system can be represented in (46) [49] either using the dynamical system or its error dynamics with a quadratic cost function, J, that needs to be minimized:

$$\begin{cases} \dot{x}(t) = Ax(t) + Bu(t) \\ J(t) = \int_0^\infty \left(x^T(t)Qx(t) + u^T(t)Ru(t) \right) dt \end{cases} \tag{46}$$

where A is the system matrix, and B is the input matrix. Most importantly, R is any positive matrix that penalizes the control efforts, u(t), and Q can be any semi-definite matrix that penalizes deviation of state vector, x(t). One outstanding feature of the LQR is that the feedback control gain, K, is calculated by solving the algebraic Ricatti formulation (ARF) of (47) [49], whose solution, P, inherently guarantees the stability of the closed-loop system. It is evident that selecting appropriate R and Q matrices is crucial as they represent the compromise between the tracking performance and the control effort. LQR has been implemented for many systems, and the calculation for the ARF is readily available in Matlab®using the *lqr(A, B, Q, R)* command. The details of using LQR for the

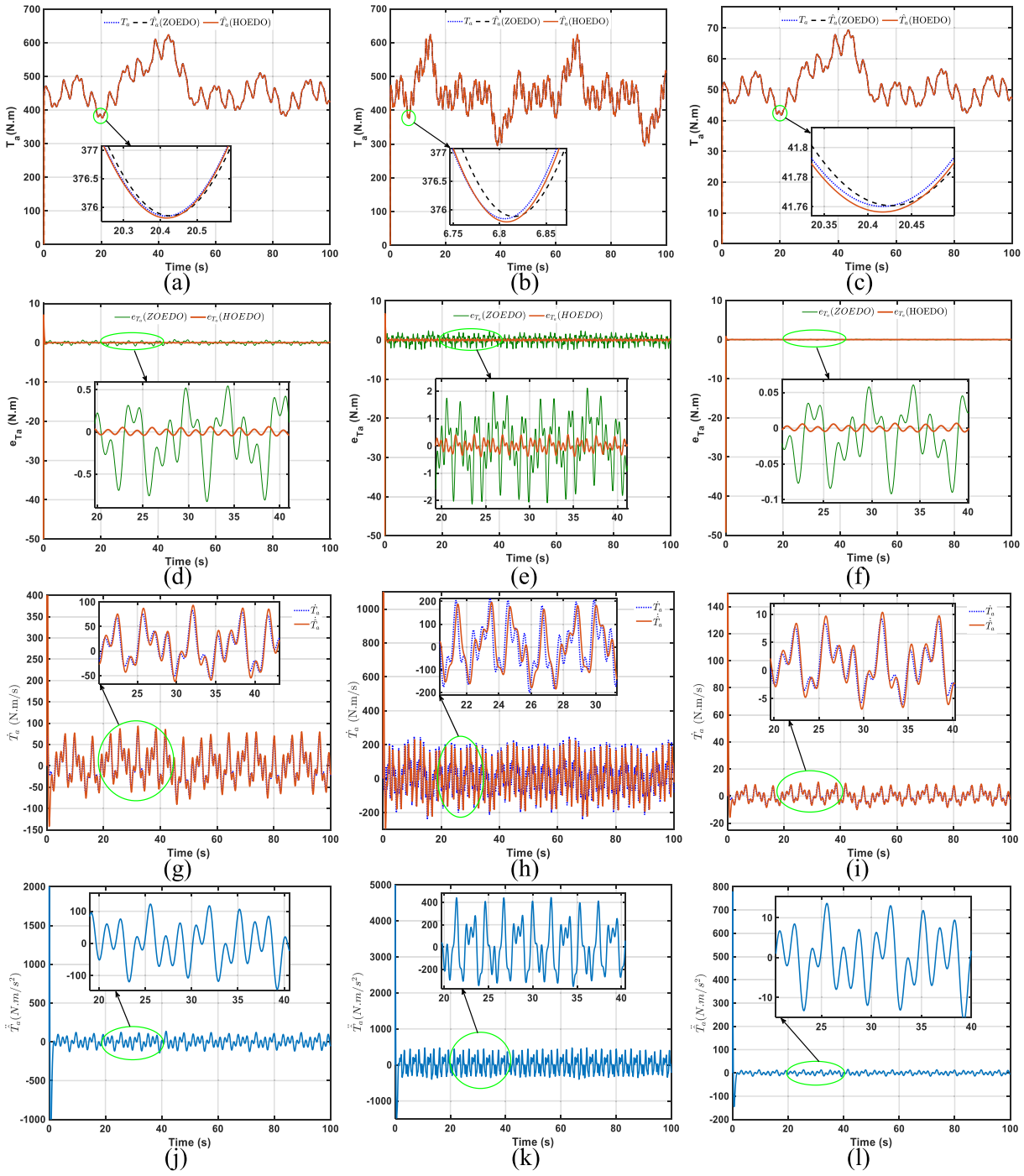

FIGURE 5. The performance of the torque estimation using HEODO and ZOEDO for the three cases of wind profiles: (a)-(c) The zero-order (ZO) torque estimation (T_a) for normal wind speed profile (Case I), increased wind frequency (Case II) and decreased wind amplitude (Case III), respectively; (d)-(f) The responses of the corresponding estimation errors for case 1, case 2, and case 3, respectively; (g)-(i) The responses for the first order (FO) torque estimation for case 1, case 2, and case 3, respectively. The responses show that the observers estimate the torques satisfactorily; (j)-(l) The responses for the second order (SO) torque estimation for case 1, case 2, and case 3, respectively. The SO torque can reach up to 400 N.m for a very fast wind profile, which could have a significant impact on the control system. Thus, the SO torque should not be neglected, especially for fast-varying wind profiles.

WECS can be found in [35], [36], and [39].

$$\begin{cases} A^T P + PA - PBR^{-1}B^T P + Q = 0 \\ K = R^{-1}B^T P \\ u(t) = -Kx(t) \end{cases} \tag{47}$$

Thus, the performance of an LQR in [39], was compared with this study. The authors used a generalized HO observer (GHOOs) for the torque estimation, while the LQR was used for the $\omega(t)$ tracking and $i_d(t)$ regulation. Although the principles and gains of the controllers were different, the simulation

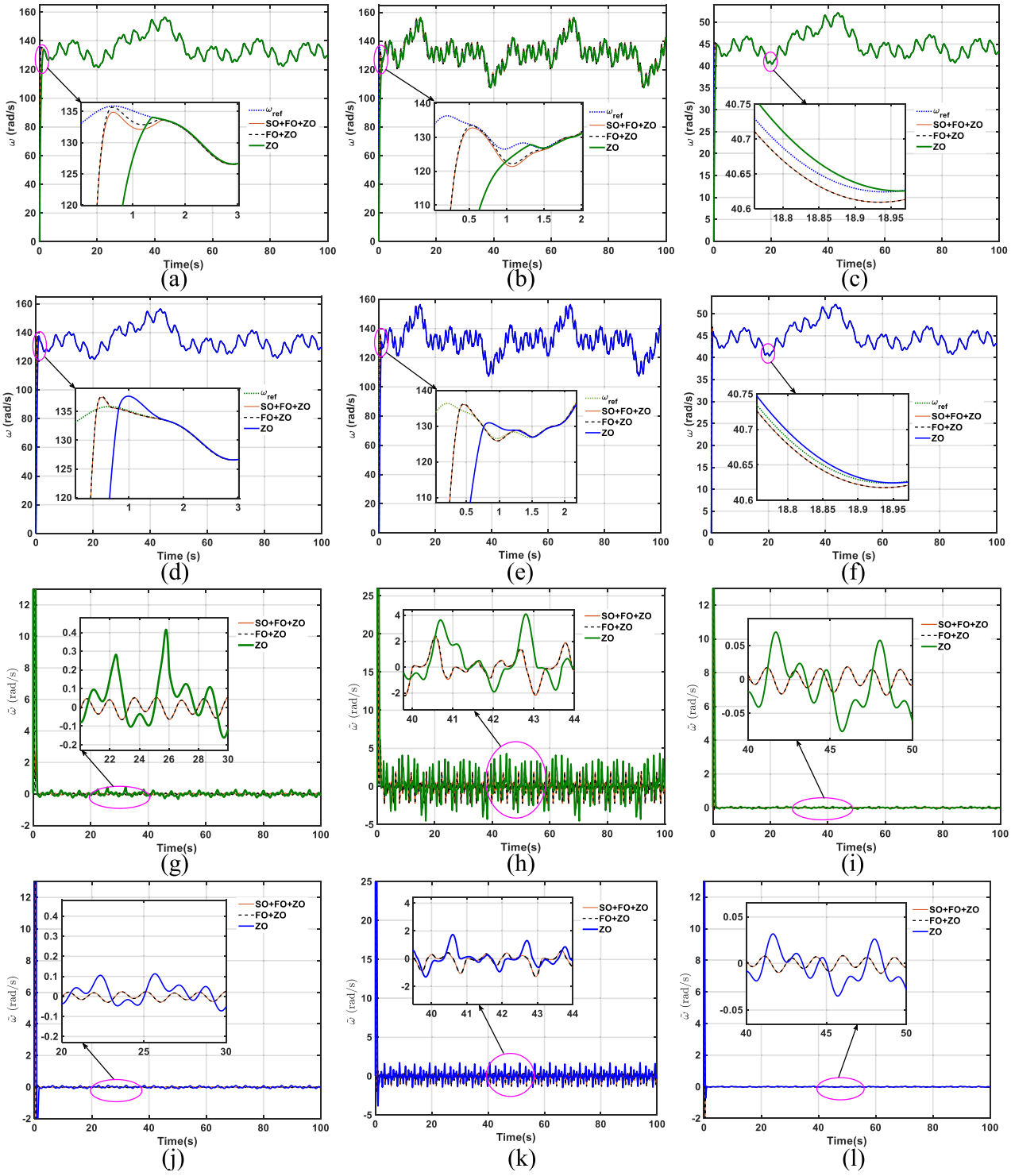

FIGURE 6. The performance of the shaft speed tracking using traditional SMC and higher-order STSMC for the three cases of wind profiles: (a)-(c) The speed (ω) tracking using SMC for normal wind speed profile (Case I), increased wind frequency (Case II) and decreased wind amplitude (Case III), respectively; (d)-(f) The ω tracking using STSMC for Case I, Case II and Case III, respectively; (g)-(i) The corresponding tracking error (ω- ω_{ref}) using SMC for case 1, case 2, and case 3, respectively; (j)-(l) The corresponding tracking error (ω- ω_{ref}) using STSMC for Case I, Case II and Case III, respectively. In each case, the STSMC demonstrated better tracking performance with minimal tracking errors than the SMC. Similarly, using ZO estimation alone demonstrated poor tracking performance as compared to adding the SO and FO estimations.

conditions of (45) and the parameters of the system of Table 1 were the same. In this regard, an objective performance comparison of the controllers could be ascertained.

Figure 8 shows the response of the proposed HOEDO-based SMC/STSMC and the GHOO-based LQR using the normal wind speed (Case I). Although both observers seem to

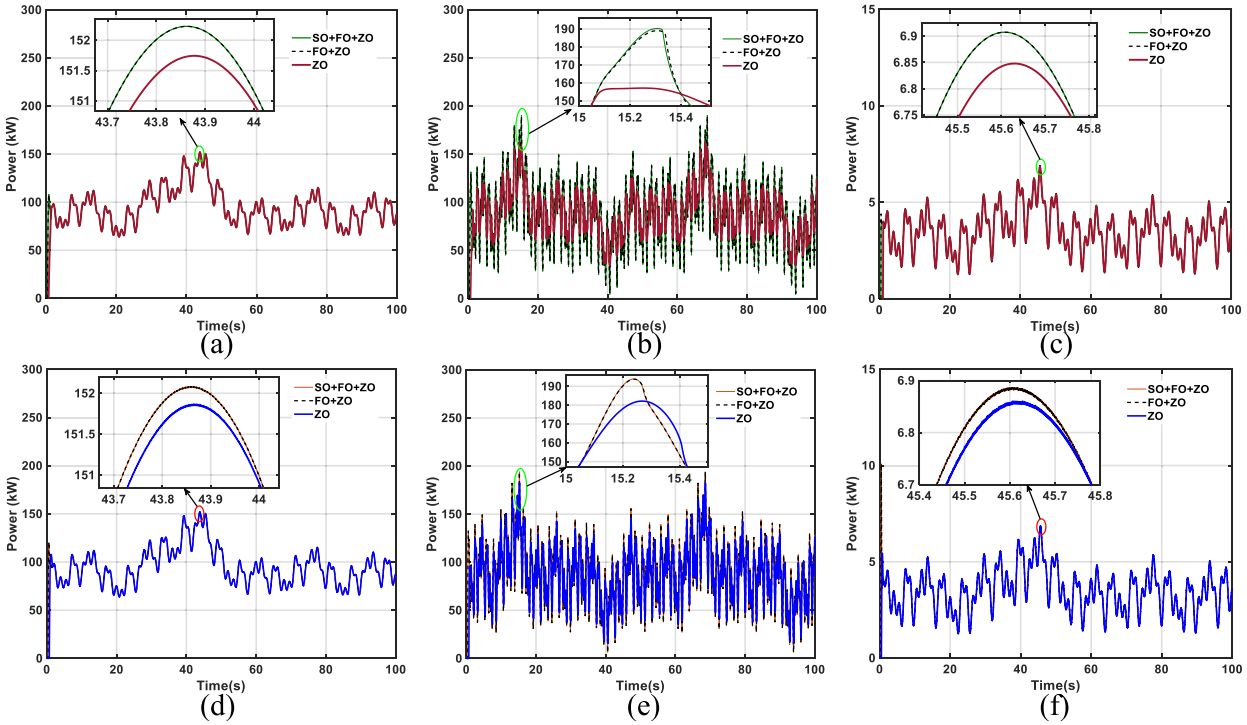

FIGURE 7. The corresponding power extraction of the WECS using HEODO and ZOEDO for the three cases of wind profiles: (a)-(c) The power harnessed using traditional SMC for normal wind speed profile (Case I), increased wind frequency (Case II) and decreased wind amplitude (Case III), respectively; (d)-(f) The power harnessed using higher-order STSMC for case 1, case 2, and case 3, respectively. Although the STSMC increased the power harnessed by using ZO, the addition of SO shows little or no improvements to the FO estimation.

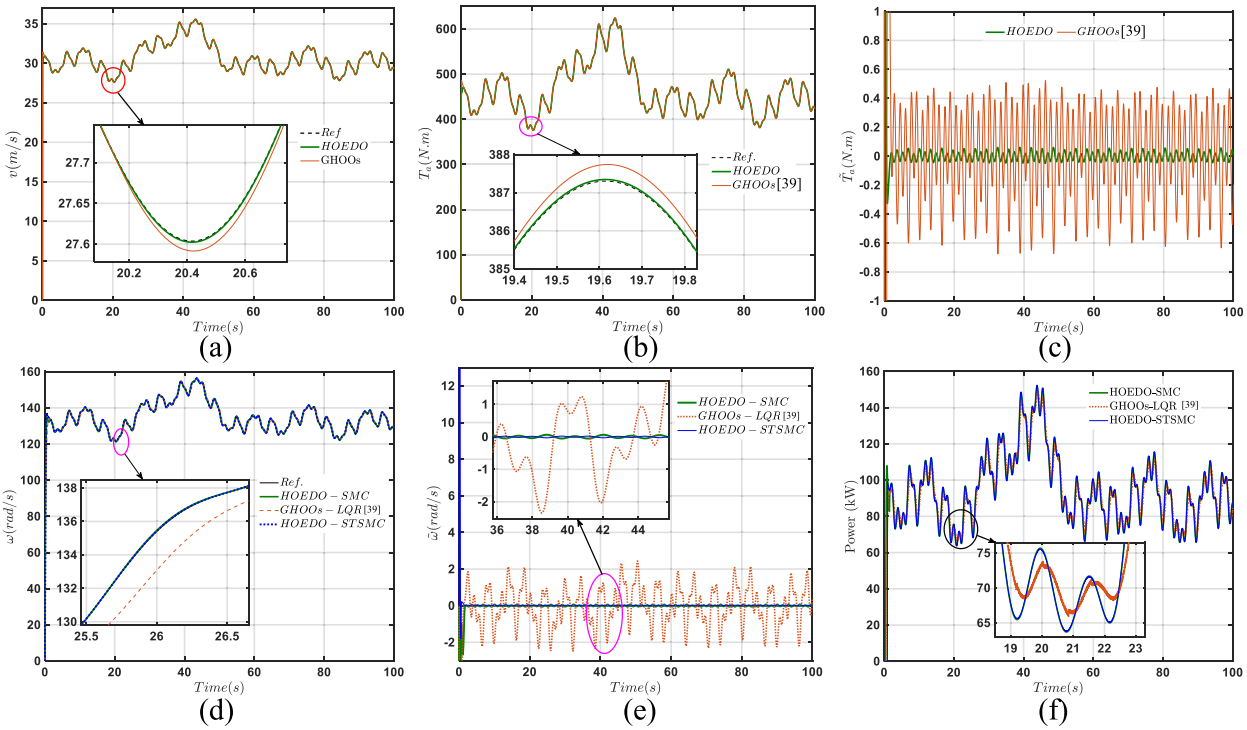

FIGURE 8. The performance comparisons for observers and controllers using normal wind speed profile (Case I). (a) Wind speed estimation; (b) Torque estimation; (c) Torque estimation error using HOEDO and GHOOs. The response demonstrated that the proposed HEODO has superior performance as compared to GHOOs [39]; (d) Speed response (ω); (e) The corresponding speed tracking error (ω- ω_{ref}) for SMC, STSMC, and LQR [39]; (f) The response of resulting power generation.

estimate the wind speed (v) and $T_a(t)$ satisfactorily, as shown in Fig. 8(a) and (b), the zoomed portion of the response demonstrated that the proposed HEODO has superior performance. Also, the Mean Absolute Error (MAE) of the

torque estimation is much smaller (better) using the HOEDO (0.1 N.m) as compared to GHOOs (0.5 N.m), as shown in Fig. 8(c). Furthermore, the performance of the three controllers was compared for the speed tracking, as shown in Fig. 8(d). The corresponding tracking error demonstrated the superior performance of the STSMC, as shown in Fig. 8(e). Similarly, the STSMC follows the reference (ω_{ref}) with a minimal tracking error of 0.22 rad/s, representing a 15% and 80% error reduction as compared to SMC (0.26 rad/s) and LQR (1.2 rad/s), respectively. Finally, the power generated using the three controllers demonstrates that the maximum power delivered by the SMC/STMC (152 kW) is about 2% higher than the power harnessed by the LQR (149 kW), as illustrated in Fig. 8(f).

Therefore, for all the performance indices, namely, $T_a(t)$ estimation, $i_d(t)$ regulation, ω(t) tracking, and power harnessing, the proposed HOEDO-based STM/SMC has outperformed the GHOO-based LQR. Unlike other studies, this study uses HOEDO for the torque estimation, and the observer and control gains of Table 2 were optimized using the gradient descent algorithm in the Matlab/Simulink optimization toolbox. Hence, the estimation and tracking performances were significantly improved.

E. ANALYSIS OF THREE-PHASE VOLTAGES AND CURRENTS

Generally, the mathematical equations of the PMSG are represented in terms of the reference rotating frame (*dq* frame). The *dq* representation is usually utilized for the control design because it simplifies the dynamics of the generator or any other machine. This scheme is made possible because the frame rotates with the magnetic fields of the rotor. Therefore, with reference to the dynamic formation of the PMSG-based WECS of (8) and the final control signals of (13) and (19)-(21), the *dq* frame needs to be converted to the actual values of the physical quantities (voltages and currents) to be measurement at the terminals of the PMSG.

Figure 9 illustrates the process of converting the signals from the *dq* to the *abc* frame. As demonstrated, the *dq* components are initially converted to $\alpha\beta$ frame using the inverse Park transformation. Then the inverse Clarke transformation is applied to convert the $\alpha\beta$ into the *abc* frames [50]. Mathematically, this can be accomplished using the formulations of (48) and (49) [51]. The transformation is also provided by a simple Matlab/Simulink block, where θ is the rotor position.

$$\begin{cases} v_\alpha = v_d \cos(\theta) - v_q \sin(\theta); \\ v_\beta = v_d \sin(\theta) + v_q \cos(\theta) \end{cases} \tag{48}$$

$$\begin{cases} v_a = v_\alpha; \\ v_b = -\dfrac{1}{2} v_\alpha + \dfrac{\sqrt{3}}{2} v_\beta; \\ v_c = -\dfrac{1}{2} v_\alpha - \dfrac{\sqrt{3}}{2} v_\beta \end{cases} \tag{49}$$

Using this transformation, the response of control signals and the corresponding three-phase supply voltages and currents for the STMC using the transformation formulations

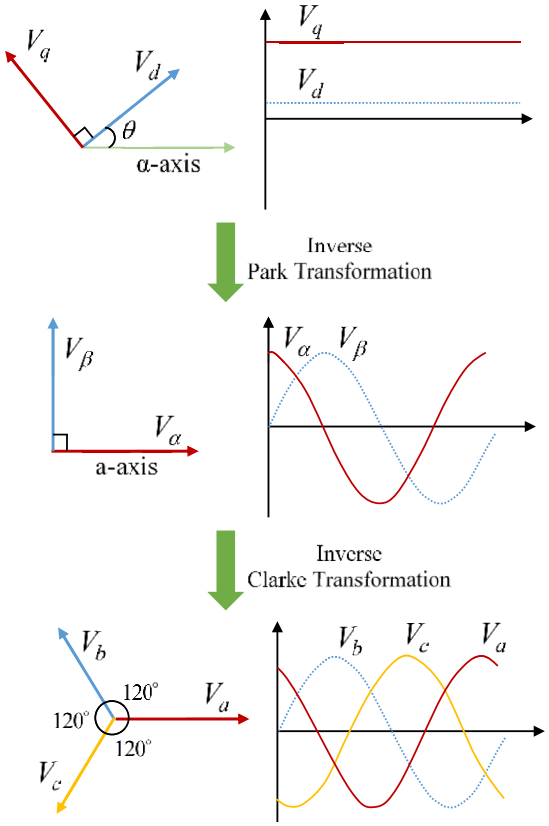

FIGURE 9. The process of converting PMSG signals to voltages and currents as physical quantities. The rotating orthogonal reference frame (dq) is converted to a two-phase orthogonal reference frame ($\alpha\beta$) using inverse Park transformation. Finally, the three-phase reference frame (abc) is obtained using inverse Clarke transformation [50].

can be assessed. On the other hand, analyzing the chattering phenomenon associated with the SMC is essential as it significantly affects the actuation (control signal). Figure 10 shows the response of the traditional SMC for the control signals (v_q and v_d) and the corresponding current (i_q). It is obvious that the traditional SMC exhibits significant chattering, which will affect the actuator and lead to unwanted noise. Therefore, unlike the SMC, the STSMC of Fig. 11 showed advanced control action with smooth control signals and current response.

VI. DISCUSSIONS

This study aimed to investigate the impact of the order of torque disturbance estimation on the control performance of PMSG-based WECS. It has been extensively studied in the literature that the wind acting on the turbine blade generates an aerodynamic torque (T_a) proportional to the wind speed and the resulting speed of the generator's shaft connected to the blades. However, the wind speed has not been effectively measured in real-time due to the fluctuating nature of the wind, which encourages sensorless torque estimation using the concept of disturbance observers. As earlier highlighted, some researchers assumed the torque to be slowly varying (zero-order), which simplifies their observer and control

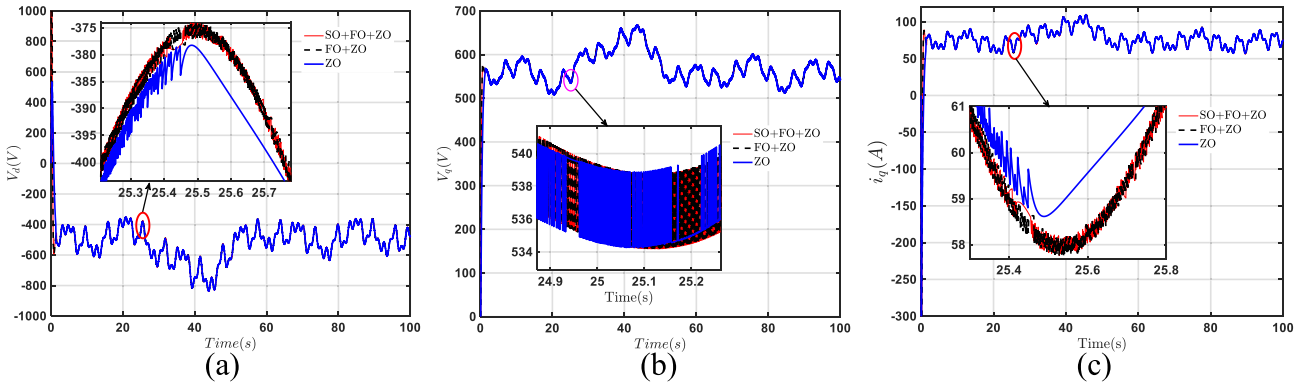

FIGURE 10. The response of control signals for the PMSG-based WECS using the traditional SMC. (a) Response d-axis voltage (v_d); (b) Response of q-axis voltage (v_q); (c) Response of q-axis current (i_q). It is clear that the SMC exhibits a lot of chattering, which can be detrimental to the system. Nonetheless, the ZO shows less chattering as compared to the HO estimations.

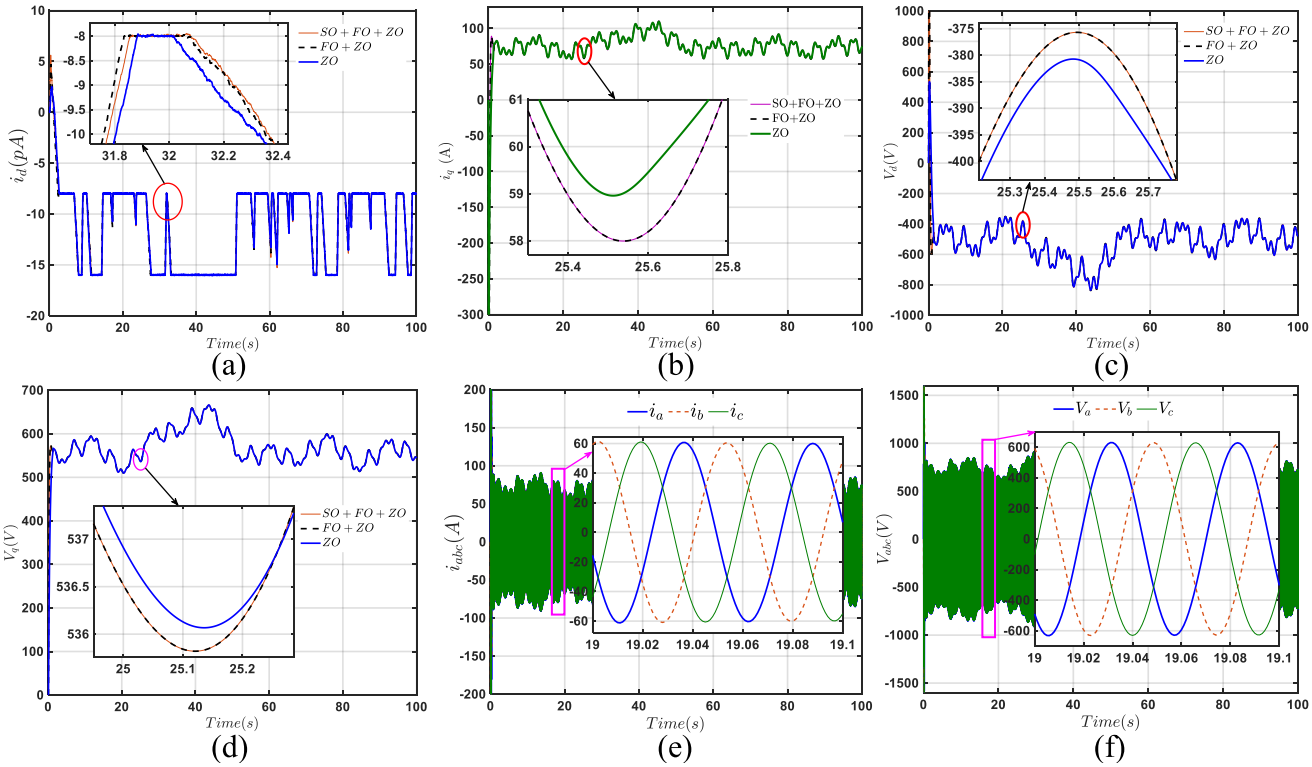

FIGURE 11. The response of converting control signals of a PSMG-based WECS (dq-frame) to three-phase physical voltages and currents (abc-frame) to be measured at the terminals of the PMSG using STSMC. (a) Response of d-axis current (i_d); (b) Response of q-axis current (i_q); (c) Response d-axis voltage (v_d); (d) Response of q-axis voltage (v_q); (e) The corresponding three-phase currents (i_{abc}); (f) The corresponding three-phase voltages (V_{abc}) using SO+FO+ZO.

design. In contrast, others claimed that the wind can fluctuate faster, and thus, the higher-order (fast-varying) torque should considered. In this study, different wind behaviors, ranging from slow to extremely varying profiles, were investigated to analyze the influence of the resulting torque on shaft speed control and the corresponding generated wind power.

In the preceding sections, three disturbance observers, namely ZO, FO, and SO, were used to control the WECS. The influence of incorporating the higher-order observers was analyzed using the three different wind profiles. Firstly, the response of the controllers with all the observers (i.e., ZO+FO+SO) was considered. Secondly, the SO estimation was considered negligible, such that the response with the ZO and FO was analyzed. Finally, only the ZO estimation was considered while neglecting the higher-order estimations (i.e., assuming a slowly varying wind profile).

Furthermore, different wind profiles were considered to study the influence of the higher-order observers

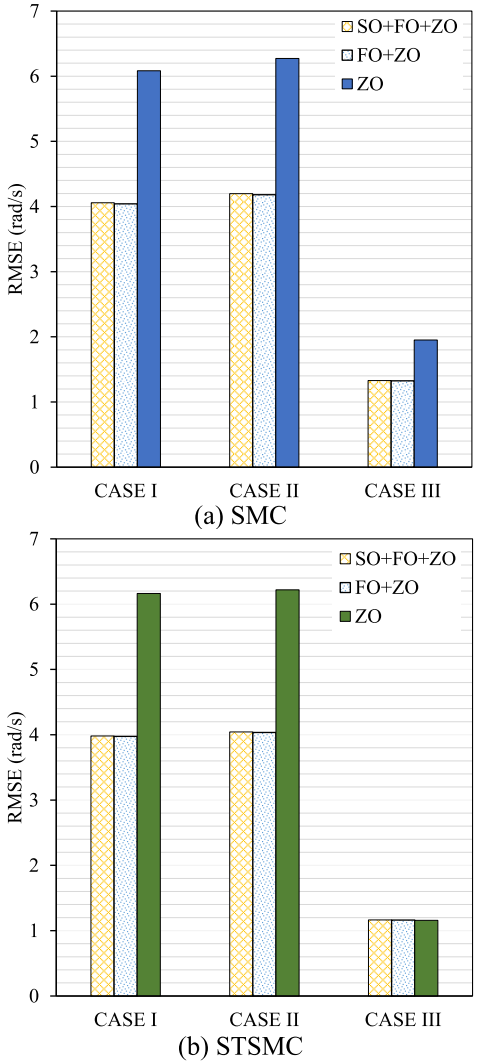

FIGURE 12. The summary of the performance indices (MAE and RMSE) of speed tracking (ω - ω_{ref}) for Case I, Case II, and Case III. (a) SMC; (b)STSMC. In all cases, the SO estimation provides insignificant improvements to the controllers. However, the ZO estimations demonstrate poor performance, especially for fast-varying wind profiles.

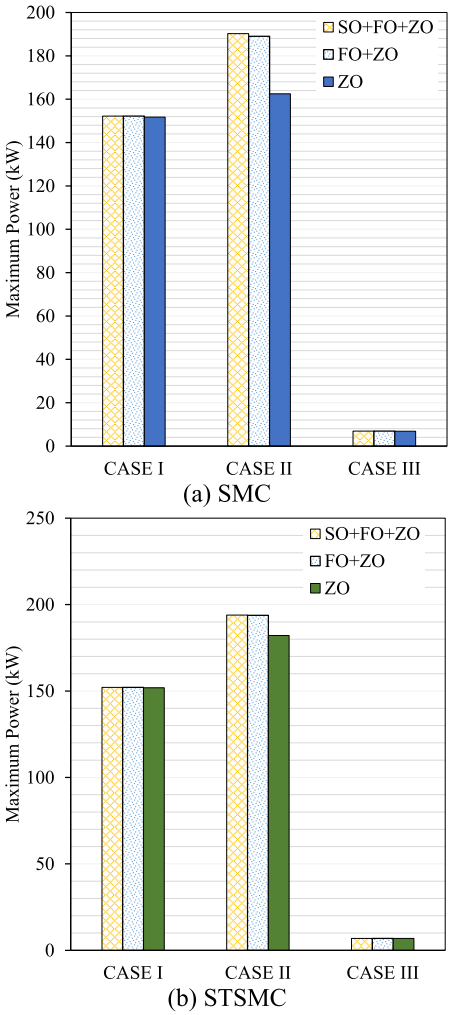

FIGURE 13. The summary of maximum power harnessed from the three wind profiles using HEODO and ZOEDO. (a) SMC; (b) STSMC. The ZO estimation satisfactorily harnessed the same amount of wind power for slow and fast varying wind profiles (Case I and III) compared to higher-order estimations (SO+FO+ZO or SO+ZO).

comprehensively. The frequency of the generated wind profile of (45) was increased threefold ($3*v_f$), and then its amplitude was decreased ($v_a/3$). The responses of the control objectives (i.e., current regulation and shaft speed tracking), disturbance estimations, and power extractions were recorded and analyzed.

The summary of the performance indices, namely mean absolute error (MAE) and root mean square error (RMSE) of the torque estimation and speed tracking were recorded. Also, the maximum power generated using SMC and STSMC is recorded, as illustrated in Table 3. It is obvious that the smaller the MAE/RMSE, the better the tracking performance of the controllers. As demonstrated, the higher the wind speed, the higher the tracking error. Nonetheless, the HOEDO has better tracking performance than the ZOEDO. It was observed that the torque estimation does not change for SMC and STSMC because the observer gains were maintained the same for the two control actions. However, the tracking error (MAE and RMSE) of STSMC shows improved performance, as illustrated in Fig. 12.

Moreover, Fig. 13 summarizes the maximum power harnessed from the three wind profiles after incorporating the observers. For Case I and III, the generated power for ZO and HO observers for both SMC/STMC were approximately the same. The results demonstrated that using the ZOEDO can almost generate the same power as the HOEDO. Nonetheless, for an extremely varying wind profile (Case II), the maximum power of 193.9 kW was extracted for the HOEDO (STSMC), representing a 6% increase as compared to 182.15 kW of the ZOEDO. The results demonstrated that HO estimations improve the speed tracking and increase the power generation of the WECS, especially for extremely changing wind profiles. On the other hand, the ZO shows satisfactory results for slow-changing wind profiles.

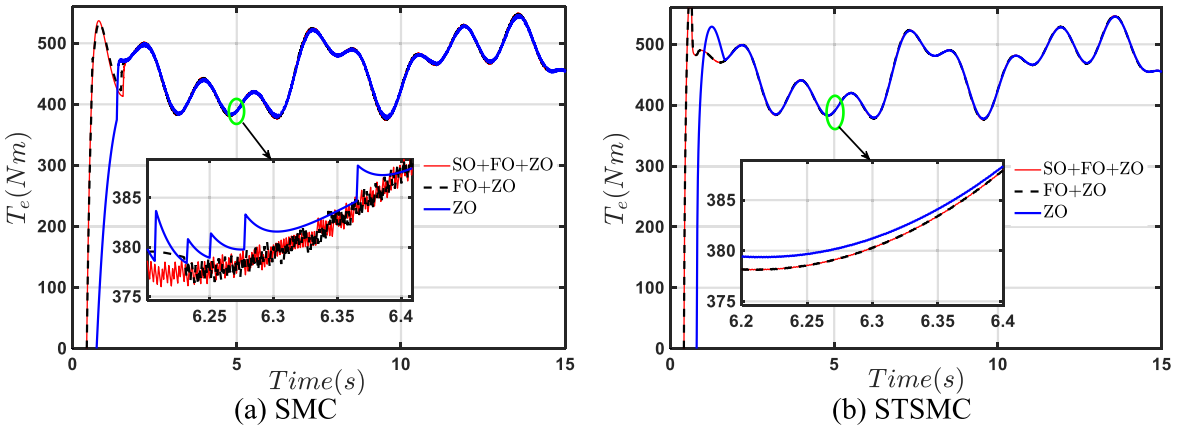

FIGURE 14. The response of electromagnetic torque (T_e), associated with the $i_q(t)$ current component for torque ripple analysis; (a) SMC; (b) ST-SMC. It is clear that the chattering effect of the traditional SMC creates some ripples, which the STSMC effectively minimizes. It is worth noting that, the torque does not oscillate but instead follows the given wind profile.

TABLE 3. Summary of torque estimation, speed tracking, and maximum power for SMC and STSMC.

Index		Scenarios	Wind profiles					
			CASE 1		CASE 2		CASE 3	
			SMC	STSMC	SMC	STSMC	SMC	STSMC
Torque Estimation Error (N.m)	MAE	HOEDO	0.0532	0.0532	0.1807	0.1807	0.0059	0.0059
		ZOEDO	0.3301	0.3301	0.8778	0.8778	0.0367	0.0367
Speed Tracking Error (ω_{ref}-ω) (rad/s)	MAE	SO+FO+ZO	0.2594	0.2151	0.8342	0.4666	0.0764	0.0566
		SO+FO	0.2495	0.2145	0.8254	0.4668	0.0759	0.0566
		ZO	0.5973	0.5061	1.6375	0.8420	0.1787	0.1044
	RMSE	SO+FO+ZO	4.0584	3.9820	4.1983	4.0431	1.3290	1.1643
		SO+FO	4.0417	3.9748	4.1809	4.0358	1.3249	1.1628
		ZO	6.0841	6.1632	6.2719	6.2193	1.9517	1.1580
Maximum power (kW)		SO+FO+ZO	152.2295	152.0847	190.2437	193.9164	6.9074	6.8871
		SO+FO	152.2291	152.0849	189.0477	193.7924	6.9074	6.8871
		ZO	151.7431	151.8682	162.4758	182.1504	6.8479	6.8604

Therefore, the study is important as it highlights the significance of torque estimation and its incorporation into the WECS's control scheme for optimal wind energy harnessing. Furthermore, the observers demonstrated that different wind profiles could be effectively estimated without the need for wind speed sensors, which reduces cost and improves the generator's shaft speed control.

On the other hand, the torques, particularly the electromagnetic torque (T_e), can exhibit ripple, which can be detrimental to the WECS. It should be noted that the study analyzes the aerodynamic torque (T_a) generated by the wind source and acts as a disturbance. However, to analyze the ripple generated by the generator, the current component is required. Thus, the $T_e(t)$ formulation of Eq. (7) was utilized to visualize the torque behavior. The analysis uses 100 seconds to capture the response of the wind profile. However, when the responses are analyzed using the zoom-in portion in the first 15 seconds of the $T_e(t)$, it is clear that the fluctuations can cause ripples for the SMC, as shown in Fig. 14(a). Interestingly, the proposed STSMC-based control ensures a smooth response without the ripple, as shown in Fig. 14(b). Most importantly, the torque does not oscillate but rather follows the given wind profile. In this study, extreme cases were analyzed for the purpose of studying the impact of extremely varying wind profiles on shaft speed control and aerodynamic torque estimation.

In summary, based on different disturbance observers (e.g., [28], [33], [34], [39], [40]) that were previously applied for torque estimation, the HEODO-based STSTMC has demonstrated superior estimation performance and ease of implementation, as extensively analyzed in Sections V and VI. The main advantage of the HEODO is that its formulation is based on the Hurwitz polynomial (Eq. (40)), which allows the observer gains to be chosen easily while ensuring guaranteed stability. The freedom of gain selection also allows the speed of error convergence to be predefined according to the control behavior and system requirements. In addition, the HEODO provides convenient integration into the controller's dynamics, which leads to improved robustness and enhanced shaft speed control accuracy.

Nonetheless, the HO estimations depend on the fast-varying nature of the wind. In this regard, the higher-frequency noise related to the variations of the wind profile will be inherently captured and amplified, especially when coupled with sensor measurement noise. Accordingly, robust and smooth control algorithms like the STSMC would be required to reject and compensate for the noise disturbances. Therefore, if the control is not robust enough, the noise will lead to estimation inaccuracies and degraded control performance.

Most importantly, when considering the practical implementation of the proposed scheme, it is imperative to note that the disturbance estimation and the STSMC are both model-dependent. In this regard, the performance of the scheme depends on the accuracy of the system parameters and the derived mathematical formulations of PSMG-based WECS. Moreover, the computational requirement regarding the response time of the observers and the control system should be considered during real-time implementation on the embedded microcontrollers. In addition, since controlling the WECS involves measurements of some quantities (e.g., generator speed, electromagnetic torque, and currents), sensor noise exists. Therefore, appropriate filters should be designed and integrated into the observer scheme to improve the signal quality and avoid noise amplification per the specifications of the available hardware setup.

VII. CONCLUSION

This paper investigates the impact of higher-order disturbance observers on the speed tracking and maximum power harnessing of WECS. The ZO, FO, and SO aerodynamic torques were estimated using the HOEDO. The results demonstrated that the HOEDO satisfactorily estimates the torque disturbance even under extremely varying wind profiles. In addition, the HOEDO-based SMC/STSMC schemes show that the d-axis current was regulated, and the shaft speed tracks the reference speed remarkably. Incorporating the disturbance estimation into the control schemes demonstrates that adding SO estimation has negligible influence on speed tracking and power extraction. It was shown that only for an extremely-varying wind profile, the HO estimation outperformed the ZO estimation for power extraction. Hence, it can be concluded that for the medium wind profile, including those described in previous research, the ZO estimation is the optimal choice, as the HO estimation showed insignificant improvement for power extraction. In addition, the FO-based STSMC has demonstrated superior performance for both shaft speed tracking and power extraction as compared to the traditional SMC in all cases of the analyzed wind profiles. The analysis shows that the proposed scheme could be satisfactorily applied for sensorless wind speed measurement and the analysis of possible wind power to be harnessed from a given wind source.

However, the main challenge for the study is that both the observers and the controllers depend on accurate dynamic modeling of the PSMG-based WECS, which might not effectively consider real-world scenarios, including nonlinearities and parameter variations due to aging or wear. In addition, when applying the proposed scheme for practical applications, the issues of sensor noise and communication delays between the control system and the sensor measurements may affect its performance. Thus, despite the advantages of the proposed scheme, there is a need for improvements, particularly during practical implementations. In this regard, our future work will focus on exploring a machine-learning-based data-driven approach with the aim of ensuring a robust control system that adapts to real-world parametric variations and other environmental uncertainties. Finally, an extensive study of the designed scheme will be conducted on a hardware-in-the-loop (HIL) setup, which mimics the practical WECS to analyze the trade-offs between computational complexity, robustness, and efficiency in real-world applications.

DECLARATION OF COMPETING INTEREST

The authors declare that they have no known competing financial interests or personal relationships that could have appeared to influence the work reported in this article.

REFERENCES

[1] A. Shalbafian and S. Ganjefar, "A novel robust nonlinear optimal second-order sliding mode control scheme for power optimization of wind energy conversion systems," *Wind Eng.*, vol. 48, no. 6, pp. 979–998, Mar. 2024, doi: 10.1177/0309524x241229403.

[2] Y. Bendjeddou, A. Deboucha, L. Bentouhami, E. Merabet, and R. Abdessemed, "Super twisting sliding mode approach applied to voltage orientated control of a stand-alone induction generator," *Protection Control Mod. Power Syst.*, vol. 6, no. 1, p. 18, Dec. 2021, doi: 10.1186/s41601-021-00201-2.

[3] A. Mansouri, A. El Magri, R. Lajouad, F. Giri, M. S. Adouairi, and B. Bossoufi, "Nonlinear observer with reduced sensors for WECS involving Vienna rectifiers–theoretical design and experimental evaluation," *Electr. Power Syst. Res.*, vol. 225, Dec. 2023, Art. no. 109847, doi: 10.1016/j.epsr.2023.109847.

[4] S. Pranupa, A. T. Sriram, and S. Nagaraja Rao, "Wind energy conversion system using perturb & observe-based maximum power point approach interfaced with T-type three-level inverter connected to grid," *Clean Energy*, vol. 6, no. 4, pp. 534–549, Aug. 2022, doi: 10.1093/ce/zkac034.

[5] B. P. Ganthia, S. K. Barik, and B. Nayak, "Wind turbines in energy conversion system: Types & techniques," in *Renewable Energy and Future Power Systems* (Energy Systems in Electrical Engineering), V. K. Singh, A. K. Bhoi, A. Saxena, A. F. Zobaa, and S. Biswal, Eds., Singapore: Springer, 2021, pp. 199–217, doi: 10.1007/978-981-33-6753-1_9.

[6] GWEC. (2023). *Global Wind Report 2023*. [Online]. Available: http://www.gwec.net/global-figures/wind-energy-global-status/

[7] Y. Kazemi and M. M. Rezaei, "A grid forming control for wind energy conversion systems," *Energy Rep.*, vol. 9, pp. 2016–2026, Dec. 2023, doi: 10.1016/j.egyr.2023.01.037.

[8] A. Sotoudeh and M. M. Rezaei, "An adaptive control strategy for grid-forming of SCIG-based wind energy conversion systems," *Energy Rep.*, vol. 10, pp. 114–122, Nov. 2023, doi: 10.1016/j.egyr.2023.06.030.

[9] S. Tyagi, B. Singh, and S. Das, "Seamless connection of wind and small hydro based energy conversion system with storage," *IEEE Trans. Ind. Appl.*, vol. 60, no. 3, pp. 4292–4301, May 2024, doi: 10.1109/tia.2024.3351114.

[10] M. S. Dall'Asta and T. B. Lazzarin, "A review of fast power-reserve control techniques in grid-connected wind energy conversion systems," *Energies*, vol. 17, no. 2, p. 451, Jan. 2024, doi: 10.3390/en17020451.

[11] M. P. Selvam, S. K. Palraj, and G. S. Madasamy, "Adaptive control of a single source reduced switch MLI-based DSTATCOM for wind energy conversion system," *Electr. Eng.*, vol. 106, no. 5, pp. 5269–5290, Jan. 2024, doi: 10.1007/s00202-023-02201-x.

[12] V. R. Rosales-Valladares, N. M. Salgado-Herrera, O. Rodríguez-Hernández, J. R. Rodríguez-Rodríguez, D. Granados-Lieberman, and O. Anaya-Lara, "Power hardware in the loop methodology applied in the integration of wind energy conversion system under fluctuations: A case study," *Energy Sour., A, Recovery, Utilization, Environ. Effects*, vol. 46, no. 1, pp. 2767–2791, Dec. 2024, doi: 10.1080/15567036.2024.2308646.

[13] R. Saulescu, C. Jaliu, M. Neagoe, D. Ciobanu, and N. Cretescu, "Comparative analysis of torque-adding wind energy conversion systems with a counter-rotating vs. Conventional electric generator," *Frontiers Energy Res.*, vol. 11, p. 1, Aug. 2023, doi: 10.3389/fenrg.2023.1215509.

[14] M. A. Mostafa, E. A. El-Hay, and M. M. Elkholy, "An overview and case study of recent low voltage ride through methods for wind energy conversion system," *Renew. Sustain. Energy Rev.*, vol. 183, Sep. 2023, Art. no. 113521, doi: 10.1016/j.rser.2023.113521.

[15] A. Chaudhuri, R. Datta, M. P. Kumar, J. P. Davim, and S. Pramanik, "Energy conversion strategies for wind energy system: Electrical, mechanical and material aspects," *Materials*, vol. 15, no. 3, p. 1232, Feb. 2022, doi: 10.3390/ma15031232.

[16] I. Lopez-Garcia, C. S. Lopez-Monsalvo, O. Gomez-Gonzalez, M. Sanabria-Villamizar, F. Beltran-Carbajal, and R. Escarela-Perez, "On the regulation of wind energy conversion systems working as conventional generation plants," *Mathematics*, vol. 11, no. 11, p. 2495, May 2023, doi: 10.3390/math11112495.

[17] J. Li, G. Wang, Z. Li, S. Yang, W. T. Chong, and X. Xiang, "A review on development of offshore wind energy conversion system," *Int. J. Energy Res.*, vol. 44, no. 12, pp. 9283–9297, Oct. 2020, doi: 10.1002/er.5751.

[18] P. Alinaghi Hosseinabadi, H. Pota, S. Mekhilef, and H. Schwartz, "Fixed-time observer-based control of DFIG-based wind energy conversion systems for maximum power extraction," *Int. J. Electr. Power Energy Syst.*, vol. 146, Mar. 2023, Art. no. 108741, doi: 10.1016/j.ijepes.2022.108741.

[19] A. S. S. Vardhan and U. K. Sinha, "Control strategies and performance analysis of doubly fed induction generator for grid-connected wind energy conversion system," *Electr. Eng.*, vol. 106, no. 2, pp. 1203–1224, Oct. 2023, doi: 10.1007/s00202-023-02079-9.

[20] B. Selma, E. Bounadja, B. Belmadani, B. Selma, and M. Fliess, "A novel intelligent control approach for wind energy conversion systems with synchronous reluctance generators," *Int. J. Circuit Theory Appl.*, vol. 52, no. 8, pp. 3967–3987, Jan. 2024, doi: 10.1002/cta.3958.

[21] A. Mseddi, K. Wali, A. Abid, O. Naifar, M. Rhaima, and L. Mchiri, "Advanced modeling and control of wind conversion systems based on hybrid generators using fractional order controllers," *Asian J. Control*, vol. 26, no. 3, pp. 1103–1119, Jan. 2024, doi: 10.1002/asjc.3282.

[22] E. Ayenew, G. Biru, A. Mulatu, and M. Berhanu, "Modelling and control of wind energy conversion system: Performance enhancement," *Int. J. Dyn. Control*, vol. 12, no. 3, pp. 891–914, Jun. 2023, doi: 10.1007/s40435-023-01201-w.

[23] S. P. Mohapatra and P. K. Dash, "A novel control strategy of a variable-speed doubly-fed-induction-generator-based wind energy conversion system," *Clean Energy*, vol. 8, no. 1, pp. 153–170, Feb. 2024, doi: 10.1093/ce/zkad074.

[24] D. Zholtayev, M. Rubagotti, and T. D. Do, "Adaptive super-twisting sliding mode control for maximum power point tracking of PMSG-based wind energy conversion systems," *Renew. Energy*, vol. 183, pp. 877–889, Jan. 2022, doi: 10.1016/j.renene.2021.11.055.

[25] X. Liu, L. Feng, X. Kong, S. Guo, and K. Y. Lee, "Tube-based stochastic model predictive control with application to wind energy conversion system," *IEEE Trans. Control Syst. Technol.*, vol. 31, no. 5, pp. 2173–2187, Sep. 2023, doi: 10.1109/TCST.2023.3291531.

[26] K. Chen, J. Lin, Y. Qiu, F. Liu, and Y. Song, "Model predictive control for wind farm power tracking with deep learning-based reduced order modeling," *IEEE Trans. Ind. Informat.*, vol. 18, no. 11, pp. 7484–7493, Nov. 2022, doi: 10.1109/TII.2022.3157302.

[27] D. Song, Z. Li, X. Deng, M. Dong, L. Huang, J. Yang, M. Su, and Y. Joo, "Deep optimization of model predictive control performance for wind turbine yaw system based on intelligent fuzzy deduction," *Expert Syst. Appl.*, vol. 221, Jul. 2023, Art. no. 119705, doi: 10.1016/j.eswa.2023.119705.

[28] T. D. Do, "Disturbance observer-based fuzzy SMC of WECSs without wind speed measurement," *IEEE Access*, vol. 5, pp. 147–155, 2017, doi: 10.1109/ACCESS.2016.2633271.

[29] H. Chen, S. Wei, W. Yang, and S. Liu, "Input wind speed forecasting for wind turbines based on spatio-temporal correlation," *Renew. Energy*, vol. 216, Nov. 2023, Art. no. 119075, doi: 10.1016/j.renene.2023.119075.

[30] M. Li, Y. Yang, Z. He, X. Guo, R. Zhang, and B. Huang, "A wind speed forecasting model based on multi-objective algorithm and interpretability learning," *Energy*, vol. 269, Apr. 2023, Art. no. 126778, doi: 10.1016/j.energy.2023.126778.

[31] B. Yan, R. Shen, K. Li, Z. Wang, Q. Yang, X. Zhou, and L. Zhang, "Spatio-temporal correlation for simultaneous ultra-short-term wind speed prediction at multiple locations," *Energy*, vol. 284, Dec. 2023, Art. no. 128418, doi: 10.1016/j.energy.2023.128418.

[32] X. Huang, C. Wang, and S. Zhang, "Research and application of a model selection forecasting system for wind speed and theoretical power generation in wind farms based on classification and wind conversion," *Energy*, vol. 293, Apr. 2024, Art. no. 130606, doi: 10.1016/j.energy.2024.130606.

[33] K. Suleimenov, B. Sarsembayev, B. Duc Hong Phuc, and T. D. Do, "Disturbance observer-based integral sliding mode control for wind energy conversion systems," *Wind Energy*, vol. 23, no. 4, pp. 1026–1047, Apr. 2020, doi: 10.1002/we.2471.

[34] J. Baran and A. Jąderko, "An MPPT control of a PMSG-based WECS with disturbance compensation and wind speed estimation," *Energies*, vol. 13, no. 23, p. 6344, Dec. 2020, doi: 10.3390/en13236344.

[35] V.-P. Vu, V.-T. Ngo, V.-D. Do, D.-N. Truong, T.-T. Huynh, and T. D. Do, "Robust MPPT observer-based control system for wind energy conversion system with uncertainties and disturbance," *IEEE Access*, vol. 9, pp. 96466–96477, 2021, doi: 10.1109/ACCESS.2021.3094819.

[36] A. Kashaganova, K. Suleimenov, S. Sagnaeva, and T. D. Do, "Maximum power tracking for wind energy conversion systems via a high-order optimal disturbance observer-based LQR without a wind speed sensor," *Eng. Sci. Technol., Int. J.*, vol. 45, Sep. 2023, Art. no. 101472, doi: 10.1016/j.jestch.2023.101472.

[37] A. B. Alhassan and T. D. Do, "Influence of higher-order disturbance estimation on maximum power extraction of wind energy conversion system using sliding mode control," in *Proc. 4th Int. Conf. Smart Grid Renew. Energy (SGRE)*, Jan. 2024, pp. 1–6, doi: 10.1109/sgre59715.2024.10428697.

[38] Y. Mousavi, G. Bevan, I. B. Kucukdemiral, and A. Fekih, "Sliding mode control of wind energy conversion systems: Trends and applications," *Renew. Sustain. Energy Rev.*, vol. 167, Oct. 2022, Art. no. 112734, doi: 10.1016/j.rser.2022.112734.

[39] A. V. Le and T. D. Do, "High-order observers-based LQ control scheme for wind speed and uncertainties estimation in WECSs," *Optim. Control Appl. Methods*, vol. 39, no. 5, pp. 1818–1832, Sep. 2018, doi: 10.1002/oca.2444.

[40] T. D. Do and H. T. Nguyen, "A generalized observer for estimating fast–varying disturbances," *IEEE Access*, vol. 6, pp. 28054–28063, 2018, doi: 10.1109/ACCESS.2018.2833430.

[41] O. C. Castillo, V. R. Andrade, J. J. R. Rivas, and R. O. González, "Comparison of power coefficients in wind turbines considering the tip speed ratio and blade pitch angle," *Energies*, vol. 16, no. 6, p. 2774, Mar. 2023, doi: 10.3390/en16062774.

[42] Y. Shtessel, C. Edwards, L. Fridman, and A. Levant, *Sliding Mode Control and Observation*. New York, NY, USA: Birkhäuser, 2014, doi: 10.1007/978-0-8176-4893-0.

[43] B. Mohapatra, B. K. Sahu, and S. Pati, "A novel optimally tuned super twisting sliding mode controller for active and reactive power control in grid-interfaced photovoltaic system," *IET Energy Syst. Integr.*, vol. 5, no. 4, pp. 491–511, Dec. 2023, doi: 10.1049/esi2.12117.

[44] T. Ito, H. Inaba, K. Kishine, M. Nakai, and K. Ishikura, "Method controlling four sets of permanent magnet synchronous motor by one inverter on a railway vehicle," in *Proc. 17th Int. Conf. Electr. Mach. Syst. (ICEMS)*, Oct. 2014, pp. 245–249, doi: 10.1109/ICEMS.2014.7013472.

[45] J. Liu. (2017). *Sliding Mode Control Using MATLAB*. [Online]. Available: https://www.elsevier.com/books-and-journals

[46] Ü. Kotta and A. Kaldmäe, "A brief tutorial overview of disturbance observers for nonlinear systems: Application to flatness-based control," *Proc. Estonian Acad. Sci.*, vol. 69, no. 1, p. 57, 2020, doi: 10.3176/proc.2020.1.07.

[47] T. Roskilly and R. Mikalsen, *Marine Systems Identification, Modeling and Control*. Oxford, U.K.: Butterworth-Heinemann, 2015, doi: 10.1016/C2013-0-18786-7.

[48] M. Zribi, M. Alrifai, and M. Rayan, "Sliding mode control of a variable-speed wind energy conversion system using a squirrel cage induction generator," *Energies*, vol. 10, no. 5, p. 604, May 2017, doi: 10.3390/en10050604.

[49] S. J. Chacko, N. P. C., and R. J. Abraham, "Optimizing LQR controllers: A comparative study," *Results Control Optim.*, vol. 14, Mar. 2024, Art. no. 100387, doi: 10.1016/j.rico.2024.100387.

[50] M. Vidlak, P. Makys, and L. Gorel, "A novel constant power factor loop for stable V/f control of PMSM in comparison against sensorless FOC with luenberger-type back-EMF observer verified by experiments," *Appl. Sci.*, vol. 12, no. 18, p. 9179, Sep. 2022, doi: 10.3390/app12189179.

[51] (2013). *Park, Inverse Park and Clarke, Inverse Clarke Software, Transformations MSS Implementation User Guide*. [Online]. Available: https://www.microsemi.com/document-portal/doc_view/132799-park-inverse-park-and-clarke-inverse-clarke-transformations-mss-software-implementation-user-guide

AHMAD BALA ALHASSAN (Member, IEEE) received the B.Eng. degree in electrical engineering from Bayero University, Kano, Nigeria, in 2011, the M.Eng. degree in mechatronics and automatic control from the University of Technology Malaysia (UTM), in 2016, and the Ph.D. degree in mechanical engineering from Xi'an Jiaotong University, China, in 2022.

He was with the Department of Mechanical Engineering, Chulalongkorn University, Thailand, as a Postdoctoral Researcher, in 2023. He is currently a Postdoctoral Scholar with the Department of Robotics and Mechatronics, Nazarbayev University, Kazakhstan. He has authored or co-authored many research articles and international conference papers on dynamic analysis and control of crane systems, inverted pendulums, rehabilitation robots, elderly-assistant robots, power transmission line inspection robots, and wind energy conversion systems. His current research interests include modeling, simulation, and control of mechatronic systems. He served as a Keynote Speaker at the 5th International Conference on Intelligent Science and Technology (ICIST 2023), Lanzhou, China. He has been a member of the IEEE Young Professionals, IEEE Control Systems Society, and the IEEE Industrial Electronics Society. He was the Technical Session Chair of the 50th IECON 2024 Conference, Chicago, IL, USA. He has also served as a Reviewer for many refereed journals, including IEEE Access, *Journal of Mechanical Science and Technology*, and *Robotics and Autonomous Systems*.

TON DUC DO (Senior Member, IEEE) received the B.S. and M.S. degrees in electrical engineering from Hanoi University of Science and Technology, Hanoi, Vietnam, in 2007 and 2009, respectively, and the Ph.D. degree in electrical engineering from Dongguk University, Seoul, South Korea, in 2014.

From 2008 to 2009, he was with the Division of Electrical Engineering, Thuy Loi University, Vietnam, as a Lecturer. He was with the Division of Electronics and Electrical Engineering, Dongguk University, as a Postdoctoral Researcher, in 2014. He was also a Senior Researcher with the Pioneer Research Center for Controlling Dementia by Converging Technology, Gyeongsang National University, South Korea, from May 2014 to August 2015. Since September 2015, he has been an Assistant Professor and an Associate Professor with the Department of Robotics and Mechatronics, Nazarbayev University, Kazakhstan. He has been listed in the top 2% of scientists based on the citation on the single-year table, since 2019, and career-wide tables, since 2021. His research interests include control engineering, electric drives, renewable energy conversion systems, and nanorobots. He received the Best Research Award from Dongguk University, in 2014, the Most Cited Paper Award from Wind Energy, in 2020 and 2021, and the Outstanding Associate Editor Award of IEEE Access, in 2021, 2022, and 2023. He received the Medal from the Minister of Science and Education of Kazakhstan for outstanding contribution to science, in 2024. He has been an Associate Editor of IEEE Access, since April 2017 and IEEE Robotics and Automation Letters, since August 2023. He has been also a Guest Editor for special issues of several journals, such as *Mathematical Problems in Engineering*, *Electronics*, *Energies*, *Sensors*, and *Fractals and Fractional*.